"Magnetic monopole" condensation of the pyrochlore ice U(1) quantum spin liquid: Application to $Pr_2Ir_2O_7$ and $Yb_2Ti_2O_7$

Gang Chen*

State Key Laboratory of Surface Physics, Center for Field Theory and Particle Physics, Department of Physics, Fudan University, Shanghai 200433, People's Republic of China

and Collaborative Innovation Center of Advanced Microstructures, Nanjing 210093, People's Republic of China

(Received 22 May 2016; revised manuscript received 6 June 2016; published 3 November 2016)

Pyrochlore iridates and pyrochlore ices are two families of materials where novel quantum phenomena are intertwined with strong spin-orbit coupling, substantial electron correlation, and geometrical frustration. Motivated by the puzzling experiments on two pyrochlore systems $Pr_2Ir_2O_7$ and $Yb_2Ti_2O_7$, we study the proximate Ising orders and the quantum phase transition out of quantum spin ice U(1) quantum spin liquid (QSL). We apply the electromagnetic duality of the compact quantum electrodynamics to analyze the condensation of the "magnetic monopoles" in the U(1) QSL. The monopole condensation naturally and necessarily leads to the Ising orders that generically break the lattice translation symmetry. We demonstrate that the antiferromagnetic Ising order with the ordering wave vector $\mathbf{Q} = 2\pi(001)$ is proximate to the U(1) QSL while the ferromagnetic Ising state with $\mathbf{Q} = (000)$ is not proximate to the U(1) QSL. This implies that if there exists a direct transition from the U(1) QSL to the ferromagnetic Ising order, the transition must be strongly first order. We apply the monopole condensation to explain the magnetic orders and the transitions in $Pr_2Ir_2O_7$ and $Yb_2Ti_2O_7$.

DOI: 10.1103/PhysRevB.94.205107

I. INTRODUCTION

Pyrochlore iridates ($R_2Ir_2O_7$) [1,2] have stimulated a wide interest in recent years, and many interesting results, including topological Mott insulator [3], quadratic band touching [4], Weyl semimetal [5–8], non-Fermi liquid [9], and so on, have been proposed. Among these materials, $Pr_2Ir_2O_7$ is of particular interest. In $Pr_2Ir_2O_7$, the Ir system remains metallic at low temperatures [10]. More intriguingly, no magnetic order was found except a partial spin freezing of the Pr local moments due to disorder at very low temperatures in the early experiments [10–12]. A recent experiment on different $Pr_2Ir_2O_7$ samples, however, discovered an antiferromagnetic long-range Ising order for the Pr moments [13]. While most theoretical works on pyrochlore iridates focused on the Ir pyrochlores and explored the interplay between the electron correlation and the strong spin-orbit coupling of the Ir $5d$ electrons [3,14], very few works considered the influence and the physics of the local moments from the rare-earth sites that also form a pyrochlore lattice [7,15–17]. In this paper, we address the local moment physics in $Pr_2Ir_2O_7$ and propose that the disordered state of the Pr moments is in the quantum spin ice (QSI) U(1) quantum spin liquid state. We explore the proximate Ising order and the confinement transition of the QSI U(1) quantum spin liquid (QSL) for the Pr local moments.

The QSI U(1) QSL is an exotic quantum phase of matter and is described by emergent compact quantum electrodynamics or, equivalently, by the compact U(1) lattice gauge theory (LGT) with a gapless U(1) gauge photon and deconfined spinon excitations [18–20]. Recently, several rare-earth pyrochlores with $4f$ electron local moments and systems alike are proposed as candidates for the QSI U(1) QSLs [21–31]. In these systems, the predominant antiferromagnetic exchange interaction between the Ising components of the local moments favors an extensively degenerate "2-in–2-out" spin ice manifold on the pyrochlore lattice [19,21,32–36]. The transverse spin interaction allows the system to tunnel quantum mechanically within the ice manifold, giving rise to a U(1) QSL ground state [35–40].

Like $Pr_2Ir_2O_7$, the experimental results on the QSI U(1) QSL candidate materials depend sensitively on the stoichiometry and the sample preparation [21]. In particular, for the pyrochlore ice system $Yb_2Ti_2O_7$, while some samples remain disordered down to the lowest temperature and the neutron scattering shows a diffusive scattering [22], others develop a ferromagnetic order [24,41–43]. This suggests that both the Yb moments in $Yb_2Ti_2O_7$ and the Pr moments in $Pr_2Ir_2O_7$ could be located near a phase transition between a disordered state [which we propose to be a QSI U(1) QSL] and the magnetic orders.

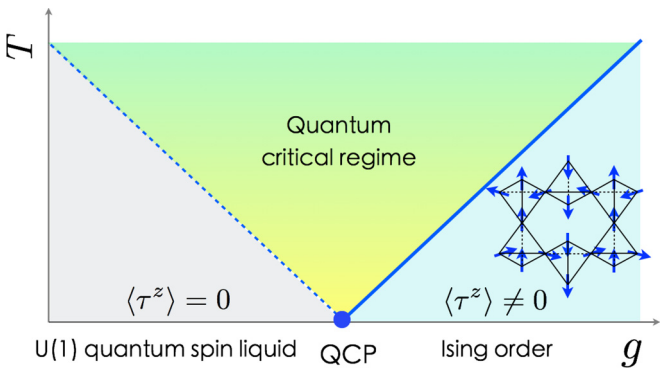

FIG. 1. The monopole condensation transition from the QSI U(1) QSL to the proximate antiferromagnetic Ising order. The dashed (solid) line represents a thermal crossover (transition). "g" is a tuning parameter that corresponds to the mass of "magnetic monopole" (see the discussion in the main text). The inset Ising order has an ordering wave vector $\mathbf{Q} = 2\pi(001)$. The Pr moment of $Pr_2Ir_2O_7$ is likely to be close to this quantum critical point (QCP).

*Corresponding author: gangchen.physics@gmail.com

On the theoretical side, the instability of the QSI U(1) QSL and the proximate magnetic orders have not been fully explored. The early works based on the gauge mean-field approach studied the instability by spinon condensation [7,37–39,44]. The spinon condensation transition, known as "Anderson-Higgs transition," generically leads to the transverse spin order that is not in the spin ice manifold [37]. Instead, we here study the proximate Ising order and transition out of the QSI U(1) QSL by condensing the "magnetic monopoles" that are topological excitations of the compact U(1) LGT for the U(1) QSL. The "magnetic monopole" used here is fundamentally distinct from the magnetic monopole in Ref. [34].[1] The monopole condensation transition is the *confinement transition* of the compact U(1) LGT [45,46], and the resulting proximate magnetic state develops an Ising order and generically breaks the lattice translation symmetry.

In $Pr_2Ir_2O_7$, the Pr^{3+} ion has a $4f^2$ electron configuration and forms a non-Kramers doublet which is represented by a pseudospin-$\frac{1}{2}$ operator $\boldsymbol{\tau}$ with τ^z (τ^x, τ^y) odd (even) under time reversal $\mathcal{T}$:

$$\mathcal{T}: \quad \tau^z \to -\tau^z, \tag{1}$$

$$\mathcal{T}: \quad \tau^{x,y} \to \tau^{x,y}. \tag{2}$$

This peculiar property under time-reversal transformation immediately indicates that the magnetic ordering of the Pr local moments *must* be signaled by the Ising component τ^z. More generally, the magnetic transition out of the QSI U(1) QSL with *any* non-Kramers doublet such as the Pr^{3+} local moments *must necessarily* be a confinement transition by the monopole condensation. The proximate Ising order, that we predict from the monopole condensation and show in Fig. 1, is *precisely* the magnetic order that has been observed by neutron diffraction in the ordered $Pr_2Ir_2O_7$ samples [13]. The Anderson-Higgs transition would, however, lead to the orderings in the transverse components. Such a transverse component order preserves the time-reversal symmetry for the non-Kramers doublets like the Pr local moments and thus does not apply to the magnetic ordering in $Pr_2Ir_2O_7$.

We extend our understanding from the monopole condensation and proximate Ising order to explain the magnetic transition in $Yb_2Ti_2O_7$. The magnetic order of $Yb_2Ti_2O_7$ preserves the lattice translation and is thus not proximate to the QSI U(1) QSL via a confinement transition. If such a magnetic state is bordering with the QSI U(1) QSL via a direct transition, the transition *must* be strongly first order. Therefore, we propose this to be the origin for the strongly first-order magnetic transition in the ordered $Yb_2Ti_2O_7$ [24,42,43].

The remaining part of the paper is organized as follows. In Sec. II, we map the low-energy theory of the relevant spin model on the pyrochlore lattice into the compact quantum electrodynamics. After carrying out an electromagnetic duality, we obtain a dual description with an explicit "magnetic monopole" degree of freedom. In Sec. III, we analyze the monopole hopping model on the dual diamond lattice and study the band structure of the monopoles. We show that the monopole condensate in the confinement phase leads to a $\mathbf{Q} = 2\pi(001)$ Ising order within the spin ice manifold. In Sec. IV, we explain the critical properties of the monopole condensation transition and emphasize the subsidiary nature of the proximate Ising order. In Sec. V, we elucidate the existing experimental results on $Pr_2Ir_2O_7$ and $Yb_2Ti_2O_7$ and make suggestions for future experiments. Finally, in the Appendixes, we provide the details of the theoretical formalism and propose a concrete spin model for the numerical verification of our prediction.

II. COMPACT QUANTUM ELECTRODYNAMICS AND ELECTROMAGNETIC DUALITY

Even though more complicated realistic Hamiltonians are available for effective spin-$\frac{1}{2}$ moments on the pyrochlore lattice [38–40], it is known that the spin-$\frac{1}{2}$ XXZ model [18]

$$H = \sum_{\langle ij \rangle} \left[J_z \tau_i^z \tau_j^z - J_\perp (\tau_i^+ \tau_j^- + \tau_i^- \tau_j^+) \right] \tag{3}$$

in the perturbative regime ($|J_\perp|/J_z \ll 1$) already captures the *universal* properties of the QSI U(1) QSL. Here, $J_z > 0$, $\tau_i^\pm \equiv \tau_i^x \pm i\tau_i^y$, and τ_i^z is defined along the local $\langle 111 \rangle$ direction of each pyrochlore site. In the perturbative regime, the third-order degenerate perturbation yields a ring exchange model [18]

$$H_{\text{ring}} = -\sum_{\hexagon_p} \frac{K}{2} (\tau_1^+ \tau_2^- \tau_3^+ \tau_4^- \tau_5^+ \tau_6^- + \text{H.c.}), \tag{4}$$

where $K = 24 J_\perp^3 / J_z^2$ and "1,...,6" are six sites on the perimeter of the elementary hexagons ("$\hexagon_p$") of the pyrochlore lattice.

To map the ring exchange model to the compact U(1) LGT, one introduces the lattice vector gauge fields as [18]

$$E_{\boldsymbol{r}\boldsymbol{r}'} \equiv \tau_i^z + \tfrac{1}{2}, \tag{5}$$

$$e^{\pm i A_{\boldsymbol{r}\boldsymbol{r}'}} \equiv \tau_i^\pm, \tag{6}$$

where the pyrochlore site i resides on the center of the nearest-neighbor diamond link $\langle \boldsymbol{r}\boldsymbol{r}' \rangle$, and $\boldsymbol{r}$ ($\boldsymbol{r}'$) is on the I (II) sublattice of the diamond lattice that is formed by the centers of the tetrahedra. Moreover, $E_{\boldsymbol{r}\boldsymbol{r}'} = -E_{\boldsymbol{r}'\boldsymbol{r}}$, $A_{\boldsymbol{r}\boldsymbol{r}'} = -A_{\boldsymbol{r}'\boldsymbol{r}}$, and $[E_{\boldsymbol{r}\boldsymbol{r}'}, A_{\boldsymbol{r}\boldsymbol{r}'}] = i$. Here, $E_{\boldsymbol{r}\boldsymbol{r}'}$ ($A_{\boldsymbol{r}\boldsymbol{r}'}$) is integer valued ($2\pi$ periodic). With this transformation, H_{ring} is transformed into the compact U(1) LGT on the diamond lattice formed by the centers of the tetrahedra

$$H_{\text{LGT}} = \sum_{\langle \boldsymbol{r}\boldsymbol{r}' \rangle} \frac{U}{2} \left(E_{\boldsymbol{r}\boldsymbol{r}'} - \frac{\epsilon_{\boldsymbol{r}}}{2} \right)^2 - \sum_{\hexagon_d} K \cos(\text{curl } A), \tag{7}$$

where we have added the electric field term with the stiffness U, $\epsilon_{\boldsymbol{r}} = +1$ (-1) for $\boldsymbol{r} \in$ I (II) sublattice, and the lattice curl ($\text{curl } A \equiv \sum_{\boldsymbol{r}\boldsymbol{r}' \in \hexagon_d} A_{\boldsymbol{r}\boldsymbol{r}'}$) defines the internal magnetic field B through the center of the diamond hexagon ($\hexagon_d$). In the large-U limit, the microscopic $\tau^z = \pm\frac{1}{2}$ is recovered. Although the actual values of U and K in the low-energy description of the U(1) QSL are renormalized from the perturbative results

[1] The latter one refers to the defect tetrahedron that has a "3-in–1-out" or "3-out–1-in" spin configuration for the classical spin ice. To distinguish them, we introduce quotation marks on the "magnetic monopole" in our context.

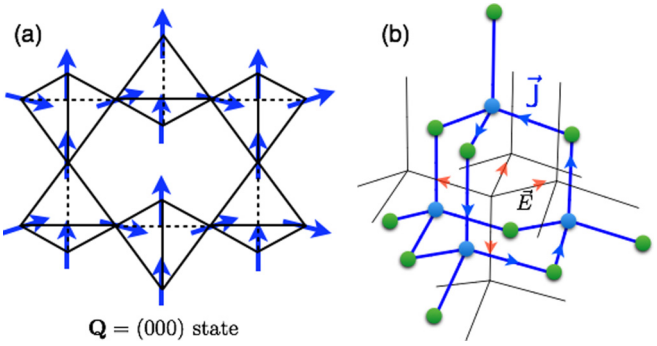

FIG. 2. (a) The $\mathbf{Q} = (000)$ ferromagnetic state. (b) The diamond lattice (in thin black) and the dual diamond lattice (in thick blue). The link of the diamond lattice goes through the center of the hexagon of the dual diamond lattice. The monopole loop current ($\vec{J}$) on the hexagon of the dual diamond lattice gives rise to the electric field ($\vec{E}$) on the link of the diamond lattice via the right hand's rule.

$H_{\rm LGT}$, that captures the universal properties of the U(1) QSI QSL [18] is the starting point of our analysis below.

"Magnetic monopoles" are topological defects of the U(1) gauge field and carry the magnetic charge. To describe the magnetic transition from the U(1) QSL via the monopole condensation, it is not so convenient to work with the field variables in Eq. (7) because the monopole variable is not explicit [18]. Instead, we apply the electromagnetic duality [18,46–50] to reformulate the compact U(1) LGT Hamiltonian and make the monopole explicit. We first introduce an integer-valued dual U(1) gauge field $a_{\mathbf{rr'}}$ that lives on the link of the dual diamond lattice (see Fig. 2) such that

$$\mathrm{curl}\, a \equiv \sum_{\mathbf{rr'}\in \hexagon_d^*} a_{\mathbf{rr'}} \equiv E_{rr'} - E^0_{rr'}, \tag{8}$$

where "$\hexagon_d^*$" refers to the elementary hexagon on the dual diamond lattice and the electric field vector $E_{rr'}$ penetrates through the center of "$\hexagon_d^*$." Here, the serif symbols $\mathbf{r},\mathbf{r'}$ label the dual diamond lattice sites. We have introduced a background electric field distribution $E^0_{rr'}$ that takes care of the background charge distribution due to the "2-in–2-out" ice rule. Each state in the spin ice manifold corresponds to a background electric field distribution. For our convenience, we choose a simple electric field configuration that corresponds to a uniform "2-in–2-out" spin ice state (see Fig. 2) with

$$E^0_{\boldsymbol{r},\boldsymbol{r}+\epsilon_r\boldsymbol{e}_0} = E^0_{\boldsymbol{r},\boldsymbol{r}+\epsilon_r\boldsymbol{e}_1} = \epsilon_r, \tag{9}$$

$$E^0_{\boldsymbol{r},\boldsymbol{r}+\epsilon_r\boldsymbol{e}_2} = E^0_{\boldsymbol{r},\boldsymbol{r}+\epsilon_r\boldsymbol{e}_3} = 0, \tag{10}$$

where $\boldsymbol{e}_\mu$ ($\mu = 0,1,2,3$) are the four vectors that connect the I sublattice sites of the diamond lattice to their nearest neighbors. In terms of the dual gauge variables, $H_{\rm LGT}$ is transformed into

$$H_{\rm dual} = \sum_{\hexagon_d^*} \frac{U}{2}(\mathrm{curl}\, a - \bar{E})^2 - \sum_{\langle \mathbf{rr'}\rangle} K\cos B_{\mathbf{rr'}}, \tag{11}$$

where we have explicitly replaced curl A with the magnetic field vector $B_{\mathbf{rr'}}$ that lives on the link $\langle \mathbf{rr'}\rangle$ of the dual diamond lattice and is conjugate to the dual gauge field a with $[B_{\mathbf{rr'}}, a_{\mathbf{rr'}}] = i$. In Eq. (11), we have introduced the electric field $\bar{E}$ that combines both the background electric field distribution E^0 and the offset in Eq. (7) with

$$\bar{E}_{\boldsymbol{r},\boldsymbol{r}+\epsilon_r\boldsymbol{e}_\mu} = E^0_{\boldsymbol{r},\boldsymbol{r}+\epsilon_r\boldsymbol{e}_\mu} - \frac{\epsilon_r}{2}. \tag{12}$$

Since the dual gauge field a is integer valued, the dual Hamiltonian $H_{\rm dual}$ is difficult to work with. Moreover, the "magnetic monopole" is implicit in the dual gauge field configuration. To make the monopole explicit, we follow the standard procedure [18,49,50] to first relax the integer-valued constraint of the dual gauge field by introducing $\cos 2\pi a$ and then insert the monopole operators. The resulting dual theory is described by the "magnetic monopoles" minimally coupled with the dual U(1) gauge field on the dual diamond lattice

$$H_{\rm dual} = \sum_{\hexagon_d^*} \frac{U}{2}(\mathrm{curl}\, a - \bar{E})^2 - \sum_{\mathbf{r},\mathbf{r'}} K\cos B_{\mathbf{rr'}} - \sum_{\langle \mathbf{r},\mathbf{r'}\rangle} t\cos(\theta_{\mathbf{r}} - \theta_{\mathbf{r'}} + 2\pi a_{\mathbf{rr'}}), \tag{13}$$

where the rotor variable $e^{-i\theta_{\mathbf{r}}}$ ($e^{i\theta_{\mathbf{r}}}$) creates (annihilates) the "magnetic monopole" at the dual lattice site $\mathbf{r}$ and $t > 0$.

III. MONOPOLE CONDENSATION AND PROXIMATE ISING ORDER

In the dual gauge Hamiltonian of Eq. (13), as the monopole hopping increases, the monopole gap decreases. When the monopole gap is closed, the monopole is condensed. In the confinement phase, the E field develops a static distribution, the B field (the a field) is strongly (weakly) fluctuating. Therefore, it is legitimate to first ignore the a field fluctuation, then study the monopole band structure, and condense the monopoles at the minimum of the monopole band for the confinement phase [49,50]. In such a dual gauge mean-field-like treatment, the "U" term in the Hamiltonian enforces $\mathrm{curl}\,\bar{a} = \bar{E}$, which is solved to fix the gauge for the dual gauge field. Here, we set the dual gauge field to its static component $\bar{a}$. The electric field distribution $\bar{E}$ turns into the dual gauge flux experienced by the "magnetic monopoles" in the dual formulation. As $\bar{E}$ takes $\pm\epsilon_r/2$, it leads to π flux of the dual gauge field through each elementary hexagon on the dual diamond lattice. As it is shown in Fig. 3, we fix the gauge by setting[2] $\bar{a}_{\mathbf{r},\mathbf{r}+\mathbf{e}_\mu} = \xi_\mu(\mathbf{q}\cdot\mathbf{r})$, where $\mathbf{r}\in$ I sublattice of the dual diamond lattice, $\mathbf{e}_\mu$ ($\mu = 0,1,2,3$) refer to the four nearest-neighbor vectors of the dual diamond lattice (see Appendix A 1), $(\xi_0,\xi_1,\xi_2,\xi_3) = (0110)$, and $\mathbf{q} = 2\pi(100)$.

In the presence of the background flux, the monopole nearest-neighbor hopping model on the dual diamond lattice is given by

$$H_m = -\sum_{\langle \mathbf{r},\mathbf{r'}\rangle} t\, e^{-i2\pi\bar{a}_{\mathbf{rr'}}}\Phi^\dagger_{\mathbf{r}}\Phi_{\mathbf{r'}} - \mu\sum_{\mathbf{r}}\Phi^\dagger_{\mathbf{r}}\Phi_{\mathbf{r}}, \tag{14}$$

[2]The gauge choice here is identical to the one used in Ref. [39] for a different problem.

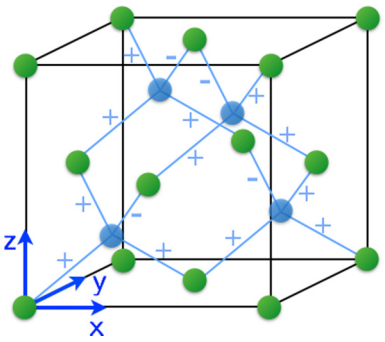

FIG. 3. The dual diamond lattice and the assignment of the gauge potential $e^{-i2\pi\tilde{a}_{\mathbf{rr}'}}$ on the nearest-neighbor links.

where we have introduced $\Phi_{\mathbf{r}} \equiv e^{i\theta_{\mathbf{r}}}$ (with $|\Phi_{\mathbf{r}}| \equiv 1$). The dispersion of the lowest monopole band is given by

$$\Omega_{\mathbf{k}} = -t[4 + 2(3 + c_{\mathsf{x}}c_{\mathsf{y}} - c_{\mathsf{x}}c_{\mathsf{z}} + c_{\mathsf{y}}c_{\mathsf{z}})^{1/2}]^{1/2} - \mu, \quad (15)$$

where $c_\mu = \cos \mathsf{k}_\mu$ ($\mu = \mathsf{x},\mathsf{y},\mathsf{z}$). The degenerate minima of the lowest band form several lines of momentum points in the Brillouin zone. One such degenerate line is along the [001] direction of the Brillouin zone and the minimum energy is $-2\sqrt{2}t - \mu$. Other degenerate lines are readily obtained by the symmetry operations. The line degeneracy of the band minima is a consequence of the background flux that frustrates the monopole hopping.

In the U(1) QSL phase, the monopole is massive and has a mass gap $-2\sqrt{2}t - \mu$. When $-2\sqrt{2}t - \mu < 0$, the monopole is condensed and the system is in the confinement phase. Since the lowest monopole dispersion has line degeneracies, we need to break the degeneracy for the monopole condensation. It is expected that the further neighbor monopole hoppings or monopole interactions should lift these degeneracies.

Due to the background flux, the lattice symmetry in H_m is realized projectively, known as projective symmetry group (PSG) [51]. We use PSG to generate the further-neighbor monopole hoppings, but do not find obvious degeneracy breaking even after including the fifth-neighbor monopole hoppings in Appendix B 2. It is possible that this degeneracy may be protected by the PSG. However, the line degeneracy immediately gets lifted if we impose the unimodular constraint on the monopole field ($|\Phi_{\mathbf{r}}| = |e^{i\theta_{\mathbf{r}}}| = 1$) after the monopole mass gap vanishes. Physically, the unimodular constraint originates from the repulsive interaction between monopoles that suppresses the density fluctuation of the monopoles. For the degenerate minima along the [001] direction, the unimodular requirement selects two equivalent momenta

$$\mathbf{k}_1 = (0,0,\pi), \quad \mathbf{k}_2 = (0,0,-\pi), \quad (16)$$

and the corresponding monopole configurations are

$$\begin{aligned} &\mathbf{r} \in \mathrm{I}, \quad \varphi_1(\mathbf{r}) = \left(\tfrac{1+i}{2} + \tfrac{1-i}{2} e^{i2\pi\mathsf{x}}\right) e^{i\pi\mathsf{z}}, \\ &\mathbf{r} \in \mathrm{II}, \quad \varphi_1(\mathbf{r}) = e^{i\pi\mathsf{z}}, \end{aligned} \quad (17)$$

$$\begin{aligned} &\mathbf{r} \in \mathrm{I}, \quad \varphi_2(\mathbf{r}) = \left(\tfrac{1-i}{2} + \tfrac{1+i}{2} e^{i2\pi\mathsf{x}}\right) e^{-i\pi\mathsf{z}}, \\ &\mathbf{r} \in \mathrm{II}, \quad \varphi_2(\mathbf{r}) = e^{-i\pi\mathsf{z}}, \end{aligned} \quad (18)$$

where φ_a refers to the monopole configuration at the momentum $\mathbf{k}_a$. Here, $\varphi_1(\mathbf{r})$ and $\varphi_2(\mathbf{r})$ are time-reversal partners. This is demanded by the time-reversal invariance of the monopole hopping Hamiltonian. From $\varphi_1(\mathbf{r})$ and $\varphi_2(\mathbf{r})$, we implement the PSG transformations and generate in total 12 symmetry-equivalent monopole configurations (see Appendix C 1).

After the unimodular constraint is enforced, the monopoles are condensed at only one of the 12 equivalent solutions, the spinons are confined, and the system develops an Ising order. Although the Ising order is induced by the monopole condensation, as monopoles are emergent particles and are not gauge invariant, the physical property of the monopole condensate is encoded in the gauge-invariant monopole bilinears. We here use symmetry to establish the relation between the spin density τ^z and the monopole bilinears. The candidate monopole bilinears are the monopole density and the monopole current. Although the monopole density ($\Phi^\dagger\Phi$) transforms in the same way as the spin density (τ^z) under the space-group symmetry, they behave oppositely under the time reversal.

As for the monopole current, from the Maxwell's equations, the loop integral of monopole current is the electric flux through the plaquette enclosed by the loop [see Fig. 2(b)] [49,50]. We have

$$\tau_i^z \sim E_{\mathbf{r}\mathbf{r}'} \sim \sum_{\mathbf{r}\mathbf{r}' \in \hexagon_d^*} \mathsf{J}_{\mathbf{r}\mathbf{r}'}, \quad (19)$$

where the pyrochlore site i is the center of the elementary hexagon $\hexagon_d^*$ on the dual diamond lattice, and

$$\mathsf{J}_{\mathbf{r}\mathbf{r}'} \equiv i[\langle\Phi_{\mathbf{r}}^\dagger\rangle\langle\Phi_{\mathbf{r}'}\rangle e^{-i\tilde{a}_{\mathbf{r}\mathbf{r}'}} - \mathrm{H.c.}] \quad (20)$$

defines the monopole current on the bond $\mathbf{r}\mathbf{r}'$. Here, $\langle\Phi_{\mathbf{r}}\rangle$ is the expectation value of the monopole field that is taken with respect to one of the 12 equivalent monopole configurations. In the inset of Fig. 1, we depict the spin density distribution of the monopole condensate at $\mathbf{k}_1$. The resulting Ising order in the confinement phase is an antiferromagnetic state with an ordering wave vector $\mathbf{Q} = 2\pi(001)$ and is in the "2-in–2-out" ice manifold. This Ising order breaks the translation symmetry by doubling the crystal unit cell. Other monopole configurations give the spin density distributions that are equivalent to the $\mathbf{Q} = 2\pi(001)$ Ising order under the space-group symmetry.

The translation symmetry breaking of the proximate Ising order is a generic phenomenon. The background gauge flux, due to the "2-in–2-out" rule, shifts the monopole band minimum to finite momenta. Once the monopole is condensed at the finite momentum, the resulting proximate Ising order necessarily breaks the translation symmetry. If the ferromagnetic Ising ordered phase with $\mathbf{Q} = (000)$ in Fig. 2(a), that preserves the translation symmetry, borders with the QSI U(1) QSL, although this Ising state is still in the ice manifold, the transition from it to the U(1) QSL must be strongly first order. In Appendix D, we propose simple spin models without a sign problem for quantum Monte Carlo simulation. The models can realize both the ferromagnetic and antiferromagnetic Ising orders and allow the careful numerical study of the phase transitions out of the QSI U(1) QSL.

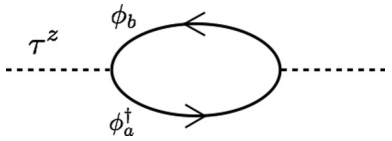

FIG. 4. The bubble diagram of the "magnetic monopole".

IV. CRITICAL THEORY OF MONOPOLE CONDENSATION

The monopole interaction in the confinement phase selects 12 equivalent monopole condensates that correspond to 12 symmetry-equivalent Ising orders. In the vicinity of the monopole condensation transition, the monopole condensate and the gauge fields fluctuate strongly. We thereby carry out a Landau-Ginzburg-Wilson expansion of the action in terms of the monopole condensate and gauge field in the vicinity of the phase transition. We introduce the slowly varying monopole fields ϕ_a via the expansion

$$\Phi_{\mathbf{r}} = \sum_{a=1}^{12} \varphi_a(\mathbf{r})\,\phi_a, \tag{21}$$

where $\varphi_a(\mathbf{r})$ $(a = 1,\ldots,12)$ are the 12 discrete monopole modes that span the ground-state manifold of the monopole condensate. With the monopole PSG, we generate the symmetry-allowed effective action for the monopole condensation transition (see Appendix C 2)

$$L = \sum_a [|(\partial_\mu - i\tilde{a}_\mu)\phi_a|^2 + m^2|\phi_a|^2] + \frac{{F_{\mu\nu}}^2}{2} + u_0 \sum_a |\phi_a|^4 + \cdots, \tag{22}$$

where we have restored the gauge field fluctuation by coupling the ϕ_a fields to the fluctuating part of the dual U(1) gauge field $\tilde{a}_\mu$, $\frac{1}{2}{F_{\mu\nu}}^2$ is the Maxwell term with $F_{\mu\nu} \equiv \partial_\mu \tilde{a}_\nu - \partial_\nu \tilde{a}_\mu$, "$\cdots$" contains further anisotropic terms that are marginal for the critical properties, m is the mass of the monopole and is set by the band gap of the monopole band structure. The effective action in Eq. (22) is a standard multicomponent Ginzburg-Landau theory in (3+1) dimensions [(3+1)D] that is the upper critical dimension of the theory. One expects the phase transition of this theory to be governed by a Gaussian fixed point or belong to a weakly first-order transition driven by fluctuations [49,50,52]. Both possibilities suggest that the mean-field treatment of the phase transition should be sufficient for a rather wide range of length scales. In a mean-field description, the monopole field correlator at the critical point (with the monopole mass $m = 0$) is

$$\langle \phi_a^\dagger(\mathbf{k}, i\omega_n)\phi_b(\mathbf{k}, i\omega_n)\rangle \sim \frac{\delta_{ab}}{\mathbf{k}^2 + \omega_n^2}. \tag{23}$$

According to Eq. (19), the spin operator is a bilinear of the monopole fields. As a result, the spin susceptibility at the ordering wave vector $\mathbf{Q}$ is simply given by the bubble diagram of monopole fields (see Fig. 4) and is thus logarithmically divergent at low temperatures with

$$\chi(\mathbf{Q}) \sim \ln \frac{1}{T}. \tag{24}$$

Such a weak divergence is a unique property of the monopole condensation transition that is a non-Landau-Ginzburg-Wilson transition. For a conventional magnetic transition, one would instead have a power-law divergence for the corresponding susceptibility. Here, the Ising order is a consequence of the monopole condensation. The condensed monopole field is the primary order, and the induced Ising order is secondary and is thus a perfect example of the subsidiary order [53,54].

The monopole mass gap controls the phase transition and is parametrized as the parameter g with $g \equiv -m^2$ in Fig. 1. In the QSI U(1) QSL phase, the monopole is massive with $m^2 > 0$. The low-energy physics is then governed by the Maxwell's field theory and the emergent gapless gauge photon. Due to the gapless photon, the heat capacity of the system behaves as $C_v \sim T^3$ at low temperatures. As the system approaches the transition from the QSL side, the monopole mass decreases. The gapless monopole at the criticality gives an extra T^3 contribution to the heat capacity. Therefore, one would observe an enhancement of the T^3 heat capacity as the system approaches the criticality. Moreover, if one raises temperatures in the U(1) QSL side, the generic argument suggests that there is no thermal phase transition except a crossover due to the thermal population of the "magnetic monopoles" [55]. The populated monopoles simply create thermal confinement of the spinons at finite temperatures. This crossover temperature is set by the mass gap of the monopoles. When $m^2 < 0$, the monopole is condensed and the system develops Ising orders. Since the system breaks time-reversal symmetry on the ordered side, we should have a finite-temperature phase transition above which the time-reversal symmetry is restored. The ordering temperature is set by the mass of the monopoles.

V. DISCUSSION

A. Transition and the Ising order in $Pr_2Ir_2O_7$

In the disordered sample of $Pr_2Ir_2O_7$, a metamagnetic transition is observed *only* for magnetic fields along the $\langle 111\rangle$ direction. This is a clear evidence that the disordered state of the Pr moments is fluctuating within the ice manifold [12,56] and the metamagnetic transition is a transition from the "2-in–2-out" ice manifold to the "3-in–1-out" manifold. Since the local moments in the QSI U(1) QSL are fluctuating quantum mechanically within the ice manifold, this metamagnetic transition in $Pr_2Ir_2O_7$ is consistent with our proposal that the disordered state of the Pr moments is a QSI U(1) QSL. In a recent measurement [56], the specific heat was found to pass the characteristic spin ice maximum and decrease until reaching a minimum at 0.4 K. At this temperature, the spin entropy approaches the Pauling value, indicating that the system enters the spin ice regime. This result again suggests that Pr local moments in disordered $Pr_2Ir_2O_7$ are fluctuating within the ice manifold.

Given the non-Kramers nature of the Pr local moment and its unique time-reversal-symmetry properties in Eqs. (1) and (2), the magnetic order of the Pr moment must be the Ising order with $\langle \tau^z \rangle \neq 0$. If a non-Kramers doublet local moment system is in a QSI U(1) QSL ground state, the magnetic transition from this state *must* be the confinement transition

of the compact U(1) LGT because a nonzero τ^z corresponds to the static electric field distribution. Remarkably, the Ising order that is found in the ordered $Pr_2Ir_2O_7$ samples by neutron diffraction [13] has an ordering wave vector $\mathbf{Q} = 2\pi(001)$, and this is precisely the proximate Ising order that we predict from the confinement transition!

In different samples, different oxygen and Ir contents shift the Fermi energy of the Ir conduction electrons and thus modify the Ruderman-Kittel-Kasuya-Yosida (RKKY) interaction between the Pr local moments [7,16,57]. This is likely to be the microscopic origin of the sample dependence. Usually, the presence of the conduction electron Fermi surface modifies the critical properties of the local moment transition. But, $Pr_2Ir_2O_7$ is very special. Due to the quadratic band touching of the Ir electrons [4,58], the Fermi energy is very close to the band touching energy and the Fermi momentum $|\mathbf{k}_F|$ is much smaller than the wave vector $\mathbf{Q}$ of the magnetic order. As a result, the particle-hole excitations of the Fermi surface of the Ir conduction electrons actually decouple from the spin fluctuations of the Pr local moments at low energies [59]. Therefore, the critical properties of the Pr local moments are not modified by the conduction electrons.

It is beneficial to focus on the disordered $Pr_2Ir_2O_7$ samples and carry out the inelastic neutron scattering. Due to the unique time-reversal-symmetry properties in Eqs. (1) and (2), only the Ising component of the Pr local moment couples with the neutron spin. As the τ^z is identified as the emergent electric field, the inelastic neutron scattering directly probes the gauge photon excitation. Because of the quadratic band touching, the inelastic neutron scattering also probes the particle-hole excitations of the Ir electrons and the spectral weight should concentrate near the Γ point. Since the energy scale of the conduction electron is much higher than the gapless gauge photon, although the spectral intensities of the low-energy gauge photon modes are peaked near the "pinch point" momenta [27,38] that are equivalent to the Γ point, it is feasible to identify the low-energy gauge photon modes in the inelastic neutron scattering measurements. It would be interesting to vary the Ir and/or oxygen contents in a continuous fashion, to drive the system between disordered and ordered phases and directly probe the phase transition.

B. Transition and the magnetic order in $Yb_2Ti_2O_7$

We first give a general discussion about the magnetic transition for the Kramers doublet. Unlike the Pr^{3+} local moment, all pseudospin components of the Kramers doublet are odd under time reversal, the magnetic transition out of the QSI U(1) QSL, that breaks the time-reversal symmetry, can be either an Anderson-Higgs transition via the spinon condensation or a confinement transition via the monopole condensation. It is well known that for the U(1) lattice gauge theory without a background electric charge distribution, the Higgs phase and the confinement phase are continuously connected [60]. For the U(1) lattice gauge theory with a background electric charge distribution, referred as "frustrated gauge theory" in the context of quantum spin ice [18,61–63], the proximate Higgs phase is actually not continuously connected to the proximate confinement phase. Depending on the "magnetic" flux that is experienced by the spinons, the Higgs phase can have a $\mathbf{Q} = 0$ order and preserves the lattice translation [38,39]. In contrast, the confinement phase orders at a finite momentum [$\mathbf{Q} = 2\pi(001)$] and breaks the lattice translation due to the background charge distribution. Therefore, if the Higgs phase preserves the translation symmetry, then there must be a translational symmetry-breaking transition as one goes from proximate Higgs phase to proximate confinement phase.

For $Yb_2Ti_2O_7$, the ordered sample has a $\mathbf{Q} = (000)$ ferromagnetic order and preserves the translation symmetry [24,41–43], although the early experiment found a disordered state [22]. The thermal transition from the high-temperature paramagnet to the ferromagnetic one is strongly first order [24,42,43]. Unlike the Pr^{3+} moment, the Yb^{3+} moment is a Kramers doublet with all pseudospin components odd under time reversal, thus, a direct coupling between τ^z and $\tau^{x,y}$ is allowed by symmetry.

In the Higgs transition scenario for $Yb_2Ti_2O_7$ [24,38,55], a predominant transverse component is induced at the first-order transition [55], and a small Ising component is induced simultaneously via the coupling between τ^z and $\tau^{x,y}$. In the scenario of a confinement transition, however, a predominant Ising order is expected, and this seems to be case in $Yb_2Ti_2O_7$ [24,42,43]. Moreover, as we have explained, the $\mathbf{Q} = (000)$ Ising order is not proximate to the QSI U(1) QSL, and the direct transition between them through monopole condensation must be strongly first order. The strongly first-order thermal transition in the ordered $Yb_2Ti_2O_7$ samples can thus be naturally regarded as a finite-temperature extension of the zero-temperature one. Therefore, it seems more natural to interpret the experiments of $Yb_2Ti_2O_7$ from the confinement scenario.

As the $\mathbf{Q} = (000)$ Ising order is not proximate to the QSI U(1) QSL, there is no sharp symmetry distinction between this state and the $\mathbf{Q} = (000)$ transverse component order for the Kramers doublet. Their connections to the U(1) QSL phase are a bit different. The direct confinement transition from the U(1) QSL to the $\mathbf{Q} = (000)$ Ising order is strongly first order even if one ignores the gauge fluctuation. The Higgs transition to the $\mathbf{Q} = (000)$ transverse component ordering is continuous in the absence of gauge fluctuation and becomes weakly first order when the gauge fluctuation is included [39,55]. Despite the absence of sharp distinction between the $\mathbf{Q} = (000)$ Ising order and the transverse component order, it is of interest to differentiate the Higgs and confinement scenarios in $Yb_2Ti_2O_7$. It would be helpful to numerically study the microscopic model [22] by varying the transverse component interaction and the Ising component interaction separately and probe the nature of transition out of the QSI U(1) QSL.

C. Summary

To summarize, we have studied the Ising magnetic orders out of the QSI U(1) QSL via the "magnetic monopole" condensation. We find that such a confinement transition gives rise to the proximate Ising ordered state that breaks the translation symmetry. We propose that the puzzling magnetic properties of $Pr_2Ir_2O_7$ and $Yb_2Ti_2O_7$ can be understood from the "magnetic monopole" condensation. Beyond these two systems, we have

argued that the magnetic transition out of the QSI U(1) QSL for a non-Kramers doublet local moments must be a confinement transition via monopole condensation. Since the Tb^{3+} local moment in $Tb_2Ti_2O_7$ is a non-Kramers doublet, it is likely that the sample-dependent magnetic order in $Tb_2Ti_2O_7$ [64] can be understood as the confinement transition. I recently became aware that the magnetic field in $Pr_2Zr_2O_7$ [65] could drive a magnetic phase transition from the thermal transport measurements. As the Pr^{3+} local moment in $Pr_2Zr_2O_7$ is a non-Kramers doublet, such a field-driven magnetic transition should be interpreted as a confinement transition.

ACKNOWLEDGMENTS

I am particularly indebted to L. Balents and G. Fiete for the clarification of their early work and the encouragement. I am especially grateful to M. P. A. Fisher for his emphasis on universality in a conversation that inspired me significantly. I acknowledge very useful conversation with C. Broholm, J. G. Cheng, X. Dai, L. Hung, Y. Kim, S. Lee, Y. Matsuda, S. Nakatsuji, T. Senthil, F. Wang, Z. Y. Weng, F. C. Zhang, and Y. Zhou and an early collaboration with M. Hermele. I sincerely thank the hospitality of O. Tchnyershov for inviting me to a pleasant trip at Johns Hopkins University where some of the insights were developed. Finally, I thank the hospitality of F. Zhang and Y. Zhou for supporting my stay at Zhejiang University. The work is supported by the Ministry of Science and Technology of People's Republic of China with the Grant No. 2016YFA0301001, the Starting-Up Fund of Fudan University (Shanghai, People's Republic of China), and the Thousand-Youth-Talent Program of People's Republic of China.

APPENDIX A: LATTICES AND SYMMETRIES

1. Pyrochlore and dual diamond lattices

Pyrochlore lattice is a corner-shared tetrahedral structure in three dimensions. The centers of the tetrahedra in the pyrochlore lattice form a diamond lattice. The dual lattice of the diamond lattice is also a diamond lattice. For the dual diamond lattice, we choose the sites

$$\mathbf{d}_1 = (0,0,0), \tag{A1}$$

$$\mathbf{d}_2 = \tfrac{1}{4}(1,1,1) \tag{A2}$$

to be the reference points of the I and II sublattices, respectively. The three lattice vectors of the underlying Bravais lattice are

$$\mathbf{a}_1 = \tfrac{1}{2}(0,1,1), \tag{A3}$$

$$\mathbf{a}_2 = \tfrac{1}{2}(1,0,1), \tag{A4}$$

$$\mathbf{a}_3 = \tfrac{1}{2}(1,1,0), \tag{A5}$$

where we have set the lattice constant to unity.

Each site of the dual diamond lattice is connected by four nearest neighbors. The four vectors $\mathbf{e}_\mu$ that connect the neighboring sites are given as

$$\mathbf{e}_0 = \tfrac{1}{4}(1,1,1), \tag{A6}$$

$$\mathbf{e}_1 = \tfrac{1}{4}(1,-1,-1), \tag{A7}$$

$$\mathbf{e}_2 = \tfrac{1}{4}(-1,1,-1), \tag{A8}$$

$$\mathbf{e}_3 = \tfrac{1}{4}(-1,-1,1). \tag{A9}$$

2. Projective symmetry group

Both the pyrochlore lattice and the dual diamond lattice share the same space-group symmetry $Fd\bar{3}m$. The $Fd\bar{3}m$ space group involves three lattice translations

$$\mathsf{T}_i : \mathbf{r} \to \mathbf{r} + \mathbf{a}_i, \tag{A10}$$

a threefold rotation

$$\mathsf{C}_3 : (\mathsf{x},\mathsf{y},\mathsf{z}) \to (\mathsf{z},\mathsf{x},\mathsf{y}), \tag{A11}$$

a twofold rotation

$$\mathsf{C}_2 : (\mathsf{x},\mathsf{y},\mathsf{z}) \to (-\mathsf{x},-\mathsf{y},\mathsf{z}), \tag{A12}$$

a mirror reflection

$$\mathsf{R} : (\mathsf{x},\mathsf{y},\mathsf{z}) \to (\mathsf{y},\mathsf{x},\mathsf{z}), \tag{A13}$$

and an inversion

$$\mathsf{I}:(\mathsf{x},\mathsf{y},\mathsf{z}) \to \left(\tfrac{1}{4}-\mathsf{x},\tfrac{1}{4}-\mathsf{y},\tfrac{1}{4}-\mathsf{z}\right). \tag{A14}$$

The physical spin is defined on the pyrochlore lattice site, while the "magnetic monopoles" are defined on the dual diamond lattice sites. Due to the background gauge flux, the space-group symmetry is realized projectively in the monopole hopping Hamiltonian H_m. For each symmetry operation, we need to supplement with a U(1) gauge transformation. Under the symmetry operation $\hat{\mathsf{O}}$, the monopole is transformed as

$$\hat{\mathsf{O}} : \Phi_{\mathbf{r}} \to e^{-i\Theta_{\mathsf{O}}(\mathbf{r})}\Phi_{\mathbf{r}'}, \tag{A15}$$

where $\mathbf{r}' = \mathsf{O}(\mathbf{r})$ and $e^{-i\Theta_{\mathsf{O}}(\mathbf{r})}$ is the associated U(1) gauge transformation. We have used $\hat{\mathsf{O}}$ to label the generator of the projective symmetry group.

For our convenience, we introduce the unit-cell index $\mathbf{n}$ to label the monopole position and define

$$\eta_1(\mathbf{n}) = \Phi_{\mathbf{r}}, \tag{A16}$$

$$\eta_2(\mathbf{n}) = \Phi_{\mathbf{r}+\mathbf{e}_0}, \tag{A17}$$

where $\mathbf{r} = \sum_j \mathsf{n}_j\mathbf{a}_j$, and $\eta_1(\mathbf{n})$ and $\eta_2(\mathbf{n})$ are monopole operators on the I and II sublattices, respectively.

Here, we list the projective symmetry transformation of the monopole operators. Under the three lattice translations, the monopole operators are transformed as

$$\hat{\mathsf{T}}_1 : \quad \eta_1(\mathsf{n}_\mathsf{x},\mathsf{n}_\mathsf{y},\mathsf{n}_\mathsf{z}) \to e^{-i\Theta_{\mathsf{T}_1}[\mathbf{n}]}\eta_1(\mathsf{n}_\mathsf{x}+1,\mathsf{n}_\mathsf{y},\mathsf{n}_\mathsf{z}), \tag{A18}$$

$$\hat{\mathsf{T}}_1 : \quad \eta_2(\mathsf{n}_\mathsf{x},\mathsf{n}_\mathsf{y},\mathsf{n}_\mathsf{z}) \to e^{-i\Theta_{\mathsf{T}_1}[\mathbf{n}]}\eta_2(\mathsf{n}_\mathsf{x}+1,\mathsf{n}_\mathsf{y},\mathsf{n}_\mathsf{z}), \tag{A19}$$

$$\hat{\mathsf{T}}_2 : \quad \eta_1(\mathsf{n}_\mathsf{x},\mathsf{n}_\mathsf{y},\mathsf{n}_\mathsf{z}) \to e^{-i\Theta_{\mathsf{T}_2}[\mathbf{n}]}\eta_1(\mathsf{n}_\mathsf{x},\mathsf{n}_\mathsf{y}+1,\mathsf{n}_\mathsf{z}), \tag{A20}$$

$$\hat{\mathsf{T}}_2 : \quad \eta_2(\mathsf{n}_\mathsf{x},\mathsf{n}_\mathsf{y},\mathsf{n}_\mathsf{z}) \to e^{-i\Theta_{\mathsf{T}_2}[\mathbf{n}]}\eta_2(\mathsf{n}_\mathsf{x},\mathsf{n}_\mathsf{y}+1,\mathsf{n}_\mathsf{z}), \tag{A21}$$

$$\hat{\mathsf{T}}_3 : \quad \eta_1(\mathsf{n}_\mathsf{x},\mathsf{n}_\mathsf{y},\mathsf{n}_\mathsf{z}) \to e^{-i\Theta_{\mathsf{T}_3}[\mathbf{n}]}\eta_1(\mathsf{n}_\mathsf{x},\mathsf{n}_\mathsf{y},\mathsf{n}_\mathsf{z}+1), \tag{A22}$$

$$\hat{\mathsf{T}}_3: \quad \eta_2(\mathsf{n_x},\mathsf{n_y},\mathsf{n_z}) \to e^{-i\Theta_{\mathsf{T}_3}[\mathbf{n}]}\eta_2(\mathsf{n_x},\mathsf{n_y},\mathsf{n_z}+1), \tag{A23}$$

where

$$\Theta_{\mathsf{T}_i}[\mathbf{n}] = -(\boldsymbol{\epsilon}\cdot\mathbf{n})\,\mathsf{v}_i \tag{A24}$$

and $\boldsymbol{\epsilon} = (1,1,0), \mathbf{v} = \pi(0,1,1)$.

Under threefold rotation, we have

$$\hat{\mathsf{C}}_3: \quad \eta_1(\mathsf{n_x},\mathsf{n_y},\mathsf{n_z}) \to e^{-i\Theta_{\mathsf{C}_3}[\mathbf{n}]}\eta_1(\mathsf{n_z},\mathsf{n_x},\mathsf{n_y}), \tag{A25}$$

$$\hat{\mathsf{C}}_3: \quad \eta_2(\mathsf{n_x},\mathsf{n_y},\mathsf{n_z}) \to e^{-i\Theta_{\mathsf{C}_3}[\mathbf{n}]}\eta_2(\mathsf{n_z},\mathsf{n_x},\mathsf{n_y}), \tag{A26}$$

where

$$\Theta_{\mathsf{C}_3}[\mathbf{n}] = \mathbf{n}\cdot\mathcal{B}\cdot\mathbf{n} + \boldsymbol{\delta}\cdot\mathbf{n} \tag{A27}$$

with

$$\mathcal{B} = \frac{\pi}{2}\begin{bmatrix} 1 & 0 & 1 \\ 0 & 1 & 1 \\ 1 & 1 & 0 \end{bmatrix} \tag{A28}$$

and $\boldsymbol{\delta} = \pi/2(1,1,0)$.

Under twofold rotation, we have

$$\hat{\mathsf{C}}_2: \quad \eta_1(\mathsf{n_x},\mathsf{n_y},\mathsf{n_z}) \to \eta_1(\mathsf{n_y},\mathsf{n_x},-\mathsf{n_x}-\mathsf{n_y}-\mathsf{n_z}), \tag{A29}$$

$$\hat{\mathsf{C}}_2: \quad \eta_2(\mathsf{n_x},\mathsf{n_y},\mathsf{n_z}) \to \eta_2(\mathsf{n_y},\mathsf{n_x},-1-\mathsf{n_x}-\mathsf{n_y}-\mathsf{n_z}), \tag{A30}$$

where $\Theta_{\mathsf{C}_2}[\mathbf{n}] = 0$.

Under the reflection, we have

$$\hat{\mathsf{R}}: \quad \eta_1(\mathsf{n_x},\mathsf{n_y},\mathsf{n_z}) \to e^{-i\Theta_{\mathsf{R}}[\mathbf{n}]}\eta_1(\mathsf{n_y},\mathsf{n_x},\mathsf{n_z}), \tag{A31}$$

$$\hat{\mathsf{R}}: \quad \eta_2(\mathsf{n_x},\mathsf{n_y},\mathsf{n_z}) \to e^{-i\Theta_{\mathsf{R}}[\mathbf{n}]}\eta_2(\mathsf{n_y},\mathsf{n_x},\mathsf{n_z}), \tag{A32}$$

where

$$\Theta_{\mathsf{R}}[\mathbf{n}] = \mathbf{n}\cdot\mathcal{B}'\cdot\mathbf{n} + \boldsymbol{\delta}'\cdot\mathbf{n} \tag{A33}$$

with

$$\mathcal{B}' = \frac{\pi}{2}\begin{bmatrix} 1 & 1 & 0 \\ 1 & 1 & 0 \\ 0 & 0 & 0 \end{bmatrix} \tag{A34}$$

and $\boldsymbol{\delta}' = \pi/2(1,1,0)$.

Finally, for the inversion symmetry, we have

$$\hat{\mathsf{I}}: \quad \eta_1(\mathsf{n_x},\mathsf{n_y},\mathsf{n_z}) \to e^{-i\Theta_{\mathsf{I}}[\mathbf{n}]}\eta_2(-\mathsf{n_x},-\mathsf{n_y},-\mathsf{n_z}), \tag{A35}$$

$$\hat{\mathsf{I}}: \quad \eta_2(\mathsf{n_x},\mathsf{n_y},\mathsf{n_z}) \to e^{-i\Theta_{\mathsf{I}}[\mathbf{n}]}\eta_1(-\mathsf{n_x},-\mathsf{n_y},-\mathsf{n_z}), \tag{A36}$$

where

$$\Theta_{\mathsf{I}}[\mathbf{n}] = \boldsymbol{\lambda}\cdot\mathbf{n} \tag{A37}$$

and $\boldsymbol{\lambda} = \pi(0,1,0)$.

APPENDIX B: MONOPOLE HOPPINGS

1. Nearest-neighbor monopole hoppings

Here, we consider the nearest-neighbor monopole hopping model. Due to the background flux and the gauge choice, the unit cell is fictitiously doubled. In Fig. 3, we specify the signs of the hopping parameters on the dual diamond lattice. The nearest-neighboring monopole hopping Hamiltonian in the momentum space is given as

$$H_m = -t\sum_{\mathbf{k}}[\Phi^\dagger_{1,1}(\mathbf{k}),\Phi^\dagger_{2,1}(\mathbf{k}),\Phi^\dagger_{1,2}(\mathbf{k}),\Phi^\dagger_{2,2}(\mathbf{k})] \times \begin{bmatrix} 0 & e^{i\mathbf{k}\cdot\mathbf{e}_0}+e^{i\mathbf{k}\cdot\mathbf{e}_1} & 0 & e^{i\mathbf{k}\cdot\mathbf{e}_2}+e^{i\mathbf{k}\cdot\mathbf{e}_3} \\ e^{-i\mathbf{k}\cdot\mathbf{e}_0}+e^{-i\mathbf{k}\cdot\mathbf{e}_1} & 0 & e^{-i\mathbf{k}\cdot\mathbf{e}_3}-e^{-i\mathbf{k}\cdot\mathbf{e}_2} & 0 \\ 0 & e^{i\mathbf{k}\cdot\mathbf{e}_3}-e^{i\mathbf{k}\cdot\mathbf{e}_2} & 0 & e^{i\mathbf{k}\cdot\mathbf{e}_0}-e^{i\mathbf{k}\cdot\mathbf{e}_1} \\ e^{-i\mathbf{k}\cdot\mathbf{e}_2}+e^{-i\mathbf{k}\cdot\mathbf{e}_3} & 0 & e^{-i\mathbf{k}\cdot\mathbf{e}_0}-e^{-i\mathbf{k}\cdot\mathbf{e}_1} & 0 \end{bmatrix} \begin{bmatrix} \Phi_{1,1}(\mathbf{k}) \\ \Phi_{2,1}(\mathbf{k}) \\ \Phi_{1,2}(\mathbf{k}) \\ \Phi_{2,2}(\mathbf{k}) \end{bmatrix} - \mu\sum_{\mu,\nu}\Phi^\dagger_{\mu,\nu}(\mathbf{k})\Phi_{\mu,\nu}(\mathbf{k}), \tag{B1}$$

where the subindex refers to the four sublattices. The reference points of the four sublattices are

$$\mathbf{d}_{1,1} = (0,0,0), \quad \mathbf{d}_{1,2} = \left(\tfrac{1}{2},\tfrac{1}{2},0\right), \tag{B2}$$

$$\mathbf{d}_{2,1} = \left(\tfrac{1}{4},\tfrac{1}{4},\tfrac{1}{4}\right), \quad \mathbf{d}_{2,2} = \left(\tfrac{3}{4},\tfrac{3}{4},\tfrac{1}{4}\right). \tag{B3}$$

Here, we define the Fourier transformation in the site basis, i.e.,

$$\text{for } \mathbf{r}\in(i,j) \text{ sublattice}, \quad \Phi(\mathbf{r}) = \sum_{\mathbf{k}}\Phi_{i,j}(\mathbf{k})e^{i\mathbf{k}\cdot\mathbf{r}}. \tag{B4}$$

The four dispersions of H_m are given as

$$\omega_{1,\pm}(\mathbf{k}) = +t\big[4\pm 2(3+\cos\mathsf{k_x}\cos\mathsf{k_y}-\cos\mathsf{k_x}\cos\mathsf{k_z} + \cos\mathsf{k_y}\cos\mathsf{k_z})^{\frac{1}{2}}\big]^{\frac{1}{2}} - \mu, \tag{B5}$$

$$\omega_{2,\pm}(\mathbf{k}) = -t\big[4\pm 2(3+\cos\mathsf{k_x}\cos\mathsf{k_y}-\cos\mathsf{k_x}\cos\mathsf{k_z} + \cos\mathsf{k_y}\cos\mathsf{k_z})^{\frac{1}{2}}\big]^{\frac{1}{2}} - \mu, \tag{B6}$$

where $\omega_{2,+}(\mathbf{k})$ is the lowest dispersion and is referred as $\Omega_{\mathbf{k}}$ in the main text.

The lowest dispersion $\omega_{2,+}(\mathbf{k})$ has line degeneracies in the momentum space. For instance, the minimum of $\omega_{2,+}(\mathbf{k})$ occurs at any momentum point along the [001] direction in the momentum space. For $\mathbf{k} = (0,0,\mathsf{k_z})$, we have the following monopole eigenstates in real space:

$$\mathbf{r}\in \mathrm{I}, \quad \Phi(\mathbf{r}) = \frac{1}{\sqrt{2}}(e^{i\frac{\mathsf{k_z}}{4}} + e^{-i\frac{\mathsf{k_z}}{4}}e^{i2\pi\mathsf{x}})e^{i\mathsf{k_z}\mathsf{z}}, \tag{B7}$$

$$\mathbf{r}\in \mathrm{II}, \quad \Phi(\mathbf{r}) = e^{i\mathsf{k_z}\mathsf{z}}. \tag{B8}$$

2. Further-neighbor monopole hoppings

The general monopole hopping model should be invariant under the PSG transformation. We here give an example for the second-neighbor monopole hopping to illustrate the procedure to determine the hopping parameters. The second neighbor connects the lattice sites within the same sublattice. Each site has 12 second-neighbor sites. For the second nearest neighbors, we consider the monopole hopping Hamiltonian

$$\begin{aligned}H_{m,2} = \sum_{\mathbf{n}} & [d_1[\mathbf{n}]\,\eta_1^\dagger(\mathsf{n_x},\mathsf{n_y},\mathsf{n_z})\eta_1(\mathsf{n_x}+1,\mathsf{n_y},\mathsf{n_z}) \\ & + d_2[\mathbf{n}]\,\eta_1^\dagger(\mathsf{n_x},\mathsf{n_y},\mathsf{n_z})\eta_1(\mathsf{n_x},\mathsf{n_y}+1,\mathsf{n_z}) \\ & + d_3[\mathbf{n}]\,\eta_1^\dagger(\mathsf{n_x},\mathsf{n_y},\mathsf{n_z})\eta_1(\mathsf{n_x},\mathsf{n_y},\mathsf{n_z}+1) \\ & + d_4[\mathbf{n}]\,\eta_1^\dagger(\mathsf{n_x},\mathsf{n_y},\mathsf{n_z})\eta_1(\mathsf{n_x},\mathsf{n_y}-1,\mathsf{n_z}+1) \\ & + d_5[\mathbf{n}]\,\eta_1^\dagger(\mathsf{n_x},\mathsf{n_y},\mathsf{n_z})\eta_1(\mathsf{n_x}-1,\mathsf{n_y},\mathsf{n_z}+1) \\ & + d_6[\mathbf{n}]\,\eta_1^\dagger(\mathsf{n_x},\mathsf{n_y},\mathsf{n_z})\eta_1(\mathsf{n_x},\mathsf{n_y}-1,\mathsf{n_z}+1) + \text{H.c.}] \\ & + [f_1[\mathbf{n}]\,\eta_2^\dagger(\mathsf{n_x},\mathsf{n_y},\mathsf{n_z})\eta_2(\mathsf{n_x}+1,\mathsf{n_y},\mathsf{n_z}) \\ & + f_2[\mathbf{n}]\,\eta_2^\dagger(\mathsf{n_x},\mathsf{n_y},\mathsf{n_z})\eta_2(\mathsf{n_x},\mathsf{n_y}+1,\mathsf{n_z}) \\ & + f_3[\mathbf{n}]\,\eta_2^\dagger(\mathsf{n_x},\mathsf{n_y},\mathsf{n_z})\eta_2(\mathsf{n_x},\mathsf{n_y},\mathsf{n_z}+1) \\ & + f_4[\mathbf{n}]\,\eta_2^\dagger(\mathsf{n_x},\mathsf{n_y},\mathsf{n_z})\eta_2(\mathsf{n_x},\mathsf{n_y}-1,\mathsf{n_z}+1) \\ & + f_5[\mathbf{n}]\,\eta_2^\dagger(\mathsf{n_x},\mathsf{n_y},\mathsf{n_z})\eta_2(\mathsf{n_x}-1,\mathsf{n_y},\mathsf{n_z}+1) \\ & + f_6[\mathbf{n}]\,\eta_2^\dagger(\mathsf{n_x},\mathsf{n_y},\mathsf{n_z})\eta_2(\mathsf{n_x}-1,\mathsf{n_y}+1,\mathsf{n_z}) + \text{H.c.}],\end{aligned} \tag{B9}$$

where $\{d_i[\mathbf{n}]\}$ and $\{f_i[\mathbf{n}]\}$ are the hopping parameters on the I and II sublattices, respectively. Applying the $\hat{\mathsf{T}}_1$ translation, we compare the transformed Hamiltonian with the original Hamiltonian and obtain

$$d_i[\mathsf{n_x},\mathsf{n_y},\mathsf{n_z}] = d_i[\mathsf{n_x}-1,\mathsf{n_y},\mathsf{n_z}]. \tag{B10}$$

Similarly, for the $\hat{\mathsf{T}}_2$ and $\hat{\mathsf{T}}_3$ translations, we have

$$d_1[\mathsf{n_x},\mathsf{n_y},\mathsf{n_z}] = -d_1[\mathsf{n_x},\mathsf{n_y}-1,\mathsf{n_z}], \tag{B11}$$

$$d_2[\mathsf{n_x},\mathsf{n_y},\mathsf{n_z}] = -d_2[\mathsf{n_x},\mathsf{n_y}-1,\mathsf{n_z}], \tag{B12}$$

$$d_3[\mathsf{n_x},\mathsf{n_y},\mathsf{n_z}] = +d_3[\mathsf{n_x},\mathsf{n_y}-1,\mathsf{n_z}], \tag{B13}$$

$$d_4[\mathsf{n_x},\mathsf{n_y},\mathsf{n_z}] = -d_4[\mathsf{n_x},\mathsf{n_y}-1,\mathsf{n_z}], \tag{B14}$$

$$d_5[\mathsf{n_x},\mathsf{n_y},\mathsf{n_z}] = -d_5[\mathsf{n_x},\mathsf{n_y}-1,\mathsf{n_z}], \tag{B15}$$

$$d_6[\mathsf{n_x},\mathsf{n_y},\mathsf{n_z}] = +d_6[\mathsf{n_x},\mathsf{n_y}-1,\mathsf{n_z}] \tag{B16}$$

and

$$d_1[\mathsf{n_x},\mathsf{n_y},\mathsf{n_z}] = -d_1[\mathsf{n_x},\mathsf{n_y},\mathsf{n_z}-1], \tag{B17}$$

$$d_2[\mathsf{n_x},\mathsf{n_y},\mathsf{n_z}] = -d_2[\mathsf{n_x},\mathsf{n_y},\mathsf{n_z}-1], \tag{B18}$$

$$d_3[\mathsf{n_x},\mathsf{n_y},\mathsf{n_z}] = +d_3[\mathsf{n_x},\mathsf{n_y},\mathsf{n_z}-1], \tag{B19}$$

$$d_4[\mathsf{n_x},\mathsf{n_y},\mathsf{n_z}] = -d_4[\mathsf{n_x},\mathsf{n_y},\mathsf{n_z}-1], \tag{B20}$$

$$d_5[\mathsf{n_x},\mathsf{n_y},\mathsf{n_z}] = -d_5[\mathsf{n_x},\mathsf{n_y},\mathsf{n_z}-1], \tag{B21}$$

$$d_6[\mathsf{n_x},\mathsf{n_y},\mathsf{n_z}] = +d_6[\mathsf{n_x},\mathsf{n_y},\mathsf{n_z}-1], \tag{B22}$$

respectively. Applying the remaining symmetries, we obtain the following hopping parameters for the second neighbors:

$$d_1[\mathsf{n_x},\mathsf{n_y},\mathsf{n_z}] = -(-)^{\mathsf{n_y}+\mathsf{n_z}}t_2, \tag{B23}$$

$$d_2[\mathsf{n_x},\mathsf{n_y},\mathsf{n_z}] = (-)^{\mathsf{n_y}+\mathsf{n_z}}t_2, \tag{B24}$$

$$d_3[\mathsf{n_x},\mathsf{n_y},\mathsf{n_z}] = -t_2, \tag{B25}$$

$$d_4[\mathsf{n_x},\mathsf{n_y},\mathsf{n_z}] = -(-)^{\mathsf{n_y}+\mathsf{n_z}}t_2, \tag{B26}$$

$$d_5[\mathsf{n_x},\mathsf{n_y},\mathsf{n_z}] = -(-)^{\mathsf{n_y}+\mathsf{n_z}}t_2, \tag{B27}$$

$$d_6[\mathsf{n_x},\mathsf{n_y},\mathsf{n_z}] = t_2. \tag{B28}$$

Here, $t_2 > 0$. The sign of t_2 is simply obtained by examining whether the triangular loop formed by two first-neighbor monopole hoppings and one second-neighbor monopole hopping in Fig. 3 traps an electric field line or not. For monopole hoppings on the II sublattice, the same procedure gives

$$f_1[\mathsf{n_x},\mathsf{n_y},\mathsf{n_z}] = -(-)^{\mathsf{n_y}+\mathsf{n_z}}t_2', \tag{B29}$$

$$f_2[\mathsf{n_x},\mathsf{n_y},\mathsf{n_z}] = (-)^{\mathsf{n_y}+\mathsf{n_z}}t_2', \tag{B30}$$

$$f_3[\mathsf{n_x},\mathsf{n_y},\mathsf{n_z}] = -t_2', \tag{B31}$$

$$f_4[\mathsf{n_x},\mathsf{n_y},\mathsf{n_z}] = (-)^{\mathsf{n_y}+\mathsf{n_z}}t_2', \tag{B32}$$

$$f_5[\mathsf{n_x},\mathsf{n_y},\mathsf{n_z}] = (-)^{\mathsf{n_y}+\mathsf{n_z}}t_2', \tag{B33}$$

$$f_6[\mathsf{n_x},\mathsf{n_y},\mathsf{n_z}] = -t_2'. \tag{B34}$$

Finally, we apply the inversion symmetry that switches two sublattices and establish $t_2' = t_2$.

Carrying out the above procedures, we proceed to generate the further-neighbor monopole hoppings up to the fifth neighbors. Both the third- and the fourth-neighbor monopole hoppings are zero. The fifth-neighbor monopole hoppings are given as

$$\begin{aligned}H_{m,5} = \sum_{\mathbf{n}} & [h_1[\mathbf{n}]\eta_1^\dagger(\mathsf{n_x},\mathsf{n_y},\mathsf{n_z})\eta_2(\mathsf{n_x}-2,\mathsf{n_y},\mathsf{n_z}) \\ & + h_2[\mathbf{n}]\eta_1^\dagger(\mathsf{n_x},\mathsf{n_y},\mathsf{n_z})\eta_2(\mathsf{n_x}-2,\mathsf{n_y},\mathsf{n_z}+1) \\ & + h_3[\mathbf{n}]\eta_1^\dagger(\mathsf{n_x},\mathsf{n_y},\mathsf{n_z})\eta_2(\mathsf{n_x}-2,\mathsf{n_y}+1,\mathsf{n_z}) \\ & + h_4[\mathbf{n}]\eta_1^\dagger(\mathsf{n_x},\mathsf{n_y},\mathsf{n_z})\eta_2(\mathsf{n_x},\mathsf{n_y}-2,\mathsf{n_z}) \\ & + h_5[\mathbf{n}]\eta_1^\dagger(\mathsf{n_x},\mathsf{n_y},\mathsf{n_z})\eta_2(\mathsf{n_x},\mathsf{n_y}-2,\mathsf{n_z}+1) \\ & + h_6[\mathbf{n}]\eta_1^\dagger(\mathsf{n_x},\mathsf{n_y},\mathsf{n_z})\eta_2(\mathsf{n_x},\mathsf{n_y},\mathsf{n_z}-2) \\ & + h_7[\mathbf{n}]\eta_1^\dagger(\mathsf{n_x},\mathsf{n_y},\mathsf{n_z})\eta_2(\mathsf{n_x},\mathsf{n_y},\mathsf{n_z}+1) \\ & + h_8[\mathbf{n}]\eta_1^\dagger(\mathsf{n_x},\mathsf{n_y},\mathsf{n_z})\eta_2(\mathsf{n_x},\mathsf{n_y}+1,\mathsf{n_z}-2) \\ & + h_9[\mathbf{n}]\eta_1^\dagger(\mathsf{n_x},\mathsf{n_y},\mathsf{n_z})\eta_2(\mathsf{n_x},\mathsf{n_y}+1,\mathsf{n_z}) \\ & + h_{10}[\mathbf{n}]\eta_1^\dagger(\mathsf{n_x},\mathsf{n_y},\mathsf{n_z})\eta_2(\mathsf{n_x}+1,\mathsf{n_y}-2,\mathsf{n_z}+1) \\ & + h_{11}[\mathbf{n}]\eta_1^\dagger(\mathsf{n_x},\mathsf{n_y},\mathsf{n_z})\eta_2(\mathsf{n_x}+1,\mathsf{n_y},\mathsf{n_z}-2) \\ & + h_{12}[\mathbf{n}]\eta_1^\dagger(\mathsf{n_x},\mathsf{n_y},\mathsf{n_z})\eta_2(\mathsf{n_x}+1,\mathsf{n_y},\mathsf{n_z}) + \text{H.c.}],\end{aligned} \tag{B35}$$

where

$$h_1[\mathsf{n_x},\mathsf{n_y},\mathsf{n_z}] = -t_5, \tag{B36}$$

$$h_2[\mathsf{n_x},\mathsf{n_y},\mathsf{n_z}] = t_5, \tag{B37}$$

$$h_3[\mathsf{n_x},\mathsf{n_y},\mathsf{n_z}] = -t_5(-)^{\mathsf{n_y}+\mathsf{n_z}}, \tag{B38}$$

$$h_4[\mathsf{n_x},\mathsf{n_y},\mathsf{n_z}] = t_5, \tag{B39}$$

$$h_5[\mathsf{n_x},\mathsf{n_y},\mathsf{n_z}] = -t_5, \tag{B40}$$

$$h_6[\mathsf{n_x},\mathsf{n_y},\mathsf{n_z}] = -t_5, \tag{B41}$$

$$h_7[\mathsf{n_x},\mathsf{n_y},\mathsf{n_z}] = -t_5, \tag{B42}$$

$$h_8[\mathsf{n_x},\mathsf{n_y},\mathsf{n_z}] = -t_5(-)^{\mathsf{n_y}+\mathsf{n_z}}, \tag{B43}$$

$$h_9[\mathsf{n_x},\mathsf{n_y},\mathsf{n_z}] = t_5(-)^{\mathsf{n_y}+\mathsf{n_z}}, \tag{B44}$$

$$h_{10}[\mathsf{n_x},\mathsf{n_y},\mathsf{n_z}] = -t_5(-)^{\mathsf{n_y}+\mathsf{n_z}}, \tag{B45}$$

$$h_{11}[\mathsf{n_x},\mathsf{n_y},\mathsf{n_z}] = t_5(-)^{\mathsf{n_y}+\mathsf{n_z}}, \tag{B46}$$

$$h_{12}[\mathsf{n_x},\mathsf{n_y},\mathsf{n_z}] = -t_5(-)^{\mathsf{n_y}+\mathsf{n_z}}, \tag{B47}$$

and $t_5 > 0$. Remarkably, the presence of second and fifth monopole hoppings does not lift the line degeneracy of $\omega_{2,+}(\mathbf{k})$. The lowest energy of the full monopole hopping Hamiltonian $H_m + H_{m,2} + H_{m,5}$ still occurs along the same momentum lines as the one for H_m. For example, along the [001] direction, the lowest energy is shifted to $\omega'(0,0,\mathsf{k_z}) = -2\sqrt{2}(t+t_5) - 4t_2 - \mu$ for an arbitrary $\mathsf{k_z}$, while the corresponding eigenstate stays the same as the one for H_m.

APPENDIX C: MONOPOLE CONDENSATES AND MAGNETIC ORDERS

1. Equivalent monopole condensates

When the monopole mass gap closes, the monopoles are condensed. As we have explained in the main text, the unimodular condition $|\Phi(\mathbf{r})| = 1$ requires the monopole fields to be condensed at $(0,0,\pm\pi)$, and the monopole configurations are given as $\varphi_1(\mathbf{r})$ and $\varphi_2(\mathbf{r})$. We here use the PSG in Appendix A 2 to generate other equivalent monopole configurations. The results are listed as follows:

$$\begin{aligned}
\mathbf{r}\in \mathrm{I}, \quad \varphi_3(\mathbf{r}) &= \frac{e^{-i\pi\mathsf{x}}}{2}(1+e^{i2\pi\mathsf{x}}+e^{i2\pi\mathsf{y}}-e^{i2\pi\mathsf{z}}),\\
\mathbf{r}\in \mathrm{II}, \quad \varphi_3(\mathbf{r}) &= \frac{e^{-i\pi\mathsf{x}}}{2}(1+e^{i2\pi\mathsf{x}}+e^{i2\pi\mathsf{y}}+ie^{i2\pi\mathsf{z}}),
\end{aligned} \tag{C1}$$

$$\begin{aligned}
\mathbf{r}\in \mathrm{I}, \quad \varphi_5(\mathbf{r}) &= \frac{1+i}{2}e^{-i\pi(\mathsf{x}+\mathsf{y}+\mathsf{z})}(-ie^{i2\pi\mathsf{x}}+e^{i2\pi\mathsf{y}}),\\
\mathbf{r}\in \mathrm{II}, \quad \varphi_5(\mathbf{r}) &= \frac{1}{2}e^{-i\pi(\mathsf{x}+\mathsf{y}+\mathsf{z})}(-i+e^{i2\pi\mathsf{x}}+ie^{i2\pi\mathsf{y}}\\
&\quad +ie^{i2\pi\mathsf{z}}),
\end{aligned} \tag{C2}$$

$$\begin{aligned}
\mathbf{r}\in \mathrm{I}, \quad \varphi_7(\mathbf{r}) &= \frac{1}{2}(i+e^{i2\pi\mathsf{y}})(-i+e^{i2\pi\mathsf{z}}),\\
\mathbf{r}\in \mathrm{II}, \quad \varphi_7(\mathbf{r}) &= \frac{1}{\sqrt{2}}(1+e^{i2\pi\mathsf{z}}),
\end{aligned} \tag{C3}$$

$$\begin{aligned}
\mathbf{r}\in \mathrm{I}, \quad \varphi_9(\mathbf{r}) &= \frac{1}{2}e^{-i\pi(\mathsf{y}+\mathsf{z})}(e^{i2\pi\mathsf{x}}+e^{i2\pi\mathsf{y}}+ie^{i2\pi\mathsf{z}}-i),\\
\mathbf{r}\in \mathrm{II}, \quad \varphi_9(\mathbf{r}) &= \frac{1+i}{2\sqrt{2}}e^{-i\pi(\mathsf{y}+\mathsf{z})}(e^{2i\pi\mathsf{x}}+e^{2i\pi\mathsf{y}}+e^{2i\pi\mathsf{z}}-i),
\end{aligned} \tag{C4}$$

$$\begin{aligned}
\mathbf{r}\in \mathrm{I}, \quad \varphi_{11}(\mathbf{r}) &= e^{i\pi(\mathsf{x}-\mathsf{y}-2\mathsf{z})},\\
\mathbf{r}\in \mathrm{II}, \quad \varphi_{11}(\mathbf{r}) &= \frac{i}{\sqrt{2}}(-1+e^{2i\pi\mathsf{x}})e^{-i\pi(\mathsf{x}+\mathsf{y}+2\mathsf{z})}.
\end{aligned} \tag{C5}$$

Finally, using time-reversal symmetry, we generate the time-reversal partners of the above monopole configurations

$$\varphi_{2n}(\mathbf{r}) = \varphi^*_{2n-1}(\mathbf{r}), \tag{C6}$$

for $n = 1,2,3,4,5,6$. Therefore, we have 12 equivalent monopole configurations.

2. Slowly varying monopole fields: Projective symmetry transformation

In Eq. (21), we expand the monopole fields $\Phi_{\mathbf{r}}$ in terms of the slowly varying fields ϕ_a's. From the symmetry properties of $\Phi_{\mathbf{r}}$, we obtain the projective symmetry transformation for the ϕ_a fields in the following. We have

$$\hat{\mathsf{T}}_1: \begin{cases}
\phi_1 \to i\phi_1, & \phi_2 \to -i\phi_2,\\
\phi_3 \to \phi_4, & \phi_4 \to \phi_3,\\
\phi_5 \to -i\phi_6, & \phi_6 \to i\phi_5,\\
\phi_7 \to \phi_8, & \phi_8 \to \phi_7,\\
\phi_9 \to -i\phi_{10}, & \phi_{10} \to i\phi_9,\\
\phi_{11} \to i\phi_{11}, & \phi_{12} \to -i\phi_{12},
\end{cases} \tag{C7}$$

$$\hat{\mathsf{T}}_2: \begin{cases}
\phi_1 \to -\phi_2, & \phi_2 \to -\phi_1,\\
\phi_3 \to i\phi_4, & \phi_4 \to -i\phi_3,\\
\phi_5 \to -i\phi_5, & \phi_6 \to i\phi_6,\\
\phi_7 \to -i\phi_7, & \phi_8 \to i\phi_8,\\
\phi_9 \to -\phi_{10}, & \phi_{10} \to -\phi_9,\\
\phi_{11} \to i\phi_{12}, & \phi_{12} \to -i\phi_{11},
\end{cases} \tag{C8}$$

$$\hat{\mathsf{T}}_3: \begin{cases}
\phi_1 \to -i\phi_2, & \phi_2 \to i\phi_1,\\
\phi_3 \to i\phi_3, & \phi_4 \to -i\phi_4,\\
\phi_5 \to \phi_6, & \phi_6 \to \phi_5,\\
\phi_7 \to -i\phi_8, & \phi_8 \to i\phi_7,\\
\phi_9 \to i\phi_9, & \phi_{10} \to -i\phi_{10},\\
\phi_{11} \to \phi_{12}, & \phi_{12} \to \phi_{11},
\end{cases} \tag{C9}$$

$$\hat{\mathsf{C}}_3: \begin{cases}
\phi_1 \to \phi_5, & \phi_2 \to \phi_6,\\
\phi_3 \to \phi_1, & \phi_4 \to \phi_2,\\
\phi_5 \to \phi_3, & \phi_6 \to \phi_4,\\
\phi_7 \to \phi_9, & \phi_8 \to \phi_{10},\\
\phi_9 \to \phi_{11}, & \phi_{10} \to \phi_{12},\\
\phi_{11} \to \phi_7, & \phi_{12} \to \phi_8,
\end{cases} \tag{C10}$$

$$\hat{\mathsf{C}}_2: \begin{cases}
\phi_1 \to \phi_1, & \phi_2 \to \phi_2,\\
\phi_3 \to \phi_4, & \phi_4 \to \phi_3,\\
\phi_5 \to \phi_6, & \phi_6 \to \phi_5,\\
\phi_7 \to \phi_7, & \phi_8 \to \phi_8,\\
\phi_9 \to \phi_{10}, & \phi_{10} \to \phi_9,\\
\phi_{11} \to \phi_{12}, & \phi_{12} \to \phi_{11},
\end{cases} \tag{C11}$$

$$\hat{\mathsf{R}}: \begin{cases} \phi_1 \to \phi_7, & \phi_2 \to \phi_8, \\ \phi_3 \to \phi_9, & \phi_4 \to \phi_{10}, \\ \phi_5 \to \phi_{11} & \phi_6 \to \phi_{12}, \\ \phi_7 \to \phi_1, & \phi_8 \to \phi_2, \\ \phi_9 \to \phi_3, & \phi_{10} \to \phi_4, \\ \phi_{11} \to \phi_5, & \phi_{12} \to \phi_6, \end{cases} \tag{C12}$$

$$\hat{\mathsf{I}}: \begin{cases} \phi_1 \to \phi_{12}, & \phi_2 \to i\phi_{11}, \\ \phi_3 \to \phi_{10}, & \phi_4 \to i\phi_9, \\ \phi_5 \to \phi_8, & \phi_6 \to i\phi_7, \\ \phi_7 \to \phi_6, & \phi_8 \to i\phi_5, \\ \phi_9 \to \phi_4, & \phi_{10} \to i\phi_3, \\ \phi_{11} \to \phi_2, & \phi_{12} \to i\phi_1. \end{cases} \tag{C13}$$

Finally, under the time-reversal symmetery $\mathcal{T}$, we have

$$\mathcal{T}: \begin{cases} \phi_1 \to \phi_1^*, & \phi_2 \to \phi_2^*, \\ \phi_3 \to \phi_3^*, & \phi_4 \to \phi_4^*, \\ \phi_5 \to \phi_5^*, & \phi_6 \to \phi_6^*, \\ \phi_7 \to \phi_7^*, & \phi_8 \to \phi_8^*, \\ \phi_9 \to \phi_9^*, & \phi_{10} \to \phi_{10}^*, \\ \phi_{11} \to \phi_{11}^*, & \phi_{12} \to \phi_{12}^*. \end{cases} \tag{C14}$$

The quartic terms in Eq. (22), that are invariant under the PSG, are given as

$$\begin{aligned} L_4 = {} & u_1[|\phi_5\phi_7|^2 + |\phi_6\phi_7|^2 + |\phi_5\phi_8|^2 + |\phi_6\phi_8|^2 + |\phi_3\phi_9|^2 + |\phi_4\phi_9|^2 + |\phi_3\phi_{10}|^2 + |\phi_4\phi_{10}|^2 + |\phi_1\phi_{11}|^2 + |\phi_2\phi_{11}|^2 \\ & + |\phi_1\phi_{12}|^2 + |\phi_2\phi_{12}|^2] + u_2[|\phi_1\phi_3|^2 + |\phi_2\phi_3|^2 + |\phi_1\phi_4|^2 + |\phi_2\phi_4|^2 + |\phi_1\phi_5|^2 + |\phi_2\phi_5|^2 + |\phi_3\phi_5|^2 + |\phi_4\phi_5|^2 \\ & + |\phi_1\phi_6|^2 + |\phi_2\phi_6|^2 + |\phi_3\phi_6|^2 + |\phi_4\phi_6|^2 + |\phi_7\phi_9|^2 + |\phi_8\phi_9|^2 + |\phi_7\phi_{10}|^2 + |\phi_8\phi_{10}|^2 + |\phi_7\phi_{11}|^2 + |\phi_8\phi_{11}|^2 + |\phi_9\phi_{11}|^2 \\ & + |\phi_{10}\phi_{11}|^2 + |\phi_7\phi_{12}|^2 + |\phi_8\phi_{12}|^2 + |\phi_9\phi_{12}|^2 + |\phi_{10}\phi_{12}|^2] + u_3[|\phi_1\phi_7|^2 + |\phi_2\phi_7|^2 + |\phi_3\phi_7|^2 + |\phi_4\phi_7|^2 + |\phi_1\phi_8|^2 \\ & + |\phi_2\phi_8|^2 + |\phi_3\phi_8|^2 + |\phi_4\phi_8|^2 + |\phi_1\phi_9|^2 + |\phi_2\phi_9|^2 + |\phi_5\phi_9|^2 + |\phi_6\phi_9|^2 + |\phi_1\phi_{10}|^2 + |\phi_2\phi_{10}|^2 + |\phi_5\phi_{10}|^2 + |\phi_6\phi_{10}|^2 \\ & + |\phi_3\phi_{11}|^2 + |\phi_4\phi_{11}|^2 + |\phi_5\phi_{11}|^2 + |\phi_6\phi_{11}|^2 + |\phi_3\phi_{12}|^2 + |\phi_4\phi_{12}|^2 + |\phi_5\phi_{12}|^2 + |\phi_6\phi_{12}|^2] + u_4[|\phi_1\phi_2|^2 + |\phi_3\phi_4|^2 \\ & + |\phi_5\phi_6|^2 + |\phi_7\phi_8|^2 + |\phi_9\phi_{10}|^2 + |\phi_{11}\phi_{12}|^2] + u_5[\phi_2^*\phi_8^*\phi_1\phi_7 - \phi_1^*\phi_8^*\phi_2\phi_7 - \phi_4^*\phi_8^*\phi_3\phi_7 - \phi_3^*\phi_8^*\phi_4\phi_7 - \phi_2^*\phi_7^*\phi_1\phi_8 \\ & + \phi_1^*\phi_7^*\phi_2\phi_8 - \phi_4^*\phi_7^*\phi_3\phi_8 - \phi_3^*\phi_7^*\phi_4\phi_8 - \phi_2^*\phi_{10}^*\phi_1\phi_9 - \phi_1^*\phi_{10}^*\phi_2\phi_9 + \phi_6^*\phi_{10}^*\phi_5\phi_9 - \phi_5^*\phi_{10}^*\phi_6\phi_9 - \phi_2^*\phi_9^*\phi_1\phi_{10} \\ & - \phi_1^*\phi_9^*\phi_2\phi_{10} - \phi_6^*\phi_9^*\phi_5\phi_{10} + \phi_5^*\phi_9^*\phi_6\phi_{10} + \phi_4^*\phi_{12}^*\phi_3\phi_{11} - \phi_3^*\phi_{12}^*\phi_4\phi_{11} - \phi_6^*\phi_{12}^*\phi_5\phi_{11} - \phi_5^*\phi_{12}^*\phi_6\phi_{11} - \phi_4^*\phi_{11}^*\phi_3\phi_{12} \\ & + \phi_3^*\phi_{11}^*\phi_4\phi_{12} - \phi_6^*\phi_{11}^*\phi_5\phi_{12} - \phi_5^*\phi_{11}^*\phi_6\phi_{12}] + u_6[\phi_{11}^*\phi_{12}^*\phi_1\phi_2 + \phi_9^*\phi_{10}^*\phi_3\phi_4 + \phi_7^*\phi_8^*\phi_5\phi_6 + \phi_5^*\phi_6^*\phi_7\phi_8 + \phi_3^*\phi_4^*\phi_9\phi_{10} \\ & + \phi_1^*\phi_2^*\phi_{11}\phi_{12}] + u_7[\phi_7^*\phi_8^*\phi_1\phi_2 + \phi_9^*\phi_{10}^*\phi_1\phi_2 + \phi_7^*\phi_8^*\phi_3\phi_4 + \phi_{11}^*\phi_{12}^*\phi_3\phi_4 + \phi_9^*\phi_{10}^*\phi_5\phi_6 + \phi_{11}^*\phi_{12}^*\phi_5\phi_6 + \phi_1^*\phi_2^*\phi_7\phi_8 \\ & + \phi_3^*\phi_4^*\phi_7\phi_8 + \phi_1^*\phi_2^*\phi_9\phi_{10} + \phi_5^*\phi_6^*\phi_9\phi_{10} + \phi_3^*\phi_4^*\phi_{11}\phi_{12} + \phi_5^*\phi_6^*\phi_{11}\phi_{12}] + u_8[\phi_3^*\phi_4^*\phi_1\phi_2 + \phi_5^*\phi_6^*\phi_1\phi_2 + \phi_1^*\phi_2^*\phi_3\phi_4 \\ & + \phi_5^*\phi_6^*\phi_3\phi_4 + \phi_1^*\phi_2^*\phi_5\phi_6 + \phi_3^*\phi_4^*\phi_5\phi_6 + \phi_9^*\phi_{10}^*\phi_7\phi_8 + \phi_{11}^*\phi_{12}^*\phi_7\phi_8 + \phi_7^*\phi_8^*\phi_9\phi_{10} + \phi_{11}^*\phi_{12}^*\phi_9\phi_{10} + \phi_7^*\phi_8^*\phi_{11}\phi_{12} \\ & + \phi_9^*\phi_{10}^*\phi_{11}\phi_{12}] + u_9[\phi_1^2(\phi_7^*)^2 - \phi_1^2(\phi_8^*)^2 + \phi_1^2(\phi_9^*)^2 + \phi_1^2(\phi_{10}^*)^2 - \phi_2^2(\phi_7^*)^2 + \phi_2^2(\phi_8^*)^2 + \phi_2^2(\phi_9^*)^2 + \phi_2^2(\phi_{10}^*)^2 + \phi_3^2(\phi_7^*)^2 \\ & + \phi_3^2(\phi_8^*)^2 + \phi_3^2(\phi_{11}^*)^2 - \phi_3^2(\phi_{12}^*)^2 + \phi_4^2(\phi_7^*)^2 + \phi_4^2(\phi_8^*)^2 - \phi_4^2(\phi_{11}^*)^2 + \phi_4^2(\phi_{12}^*)^2 + \phi_5^2(\phi_9^*)^2 - \phi_5^2(\phi_{10}^*)^2 + \phi_5^2(\phi_{11}^*)^2 \\ & + \phi_5^2(\phi_{12}^*)^2 - \phi_6^2(\phi_9^*)^2 + \phi_6^2(\phi_{10}^*)^2 + \phi_6^2(\phi_{11}^*)^2 + \phi_6^2(\phi_{12}^*)^2 + \phi_7^2(\phi_1^*)^2 - \phi_7^2(\phi_2^*)^2 + \phi_7^2(\phi_3^*)^2 + \phi_7^2(\phi_4^*)^2 - \phi_8^2(\phi_1^*)^2 \\ & + \phi_8^2(\phi_2^*)^2 + \phi_8^2(\phi_3^*)^2 + \phi_8^2(\phi_4^*)^2 + \phi_9^2(\phi_1^*)^2 + \phi_9^2(\phi_2^*)^2 + \phi_9^2(\phi_5^*)^2 - \phi_9^2(\phi_6^*)^2 + \phi_{10}^2(\phi_1^*)^2 + \phi_{10}^2(\phi_2^*)^2 - \phi_{10}^2(\phi_5^*)^2 \\ & + \phi_{10}^2(\phi_6^*)^2 + \phi_{11}^2(\phi_3^*)^2 - \phi_{11}^2(\phi_4^*)^2 + \phi_{11}^2(\phi_5^*)^2 + \phi_{11}^2(\phi_6^*)^2 - \phi_{12}^2(\phi_3^*)^2 + \phi_{12}^2(\phi_4^*)^2 + \phi_{12}^2(\phi_5^*)^2 + \phi_{12}^2(\phi_6^*)^2] + u_0 \sum_a |\phi_a|^4. \end{aligned} \tag{C15}$$

APPENDIX D: A SIGN-PROBLEM-FREE MODEL FOR QUANTUM MONTE CARLO SIMULATION

Here, we propose a simple exchange model that does not have a sign problem for quantum Monte Carlo (QMC) simulation. This model can realize both the $\mathbf{Q} = 2\pi(001)$ order and the $\mathbf{Q} = (000)$ order. Although both Ising orders belong to the spin ice manifold, the former is proximate to the QSI U(1) QSL via a confinement transition and the latter is not (see the main text for the detailed discussion). The model is given as

$$H_1 = \sum_{\langle ij \rangle} J_z \tau_i^z \tau_j^z - J_\perp(\tau_i^+ \tau_j^- + \text{H.c.}) + \sum_{\langle\langle\langle ij \rangle\rangle\rangle} J_{3z} \tau_i^z \tau_j^z, \tag{D1}$$

where J_{3z} is the third-neighbor Ising exchange. The XXZ part of the model ($J_{3z} = 0$) has been studied in the previous works [66–68].

We focus our discussion on the case when $J_\perp > 0$. This is precisely the parameter regime where the sign problem for QMC is absent. To be in the spin ice regime, we keep $J_z > 0$. When $J_\pm \ll J_z$ and $J_{3z} \ll J_z$, the ground state is a QSI U(1) QSL. If we fix $J_\pm/J_z$ to make the system in the QSI U(1) QSL phase, as we gradually increase $|J_{3z}/J_z|$ from 0, the system will eventually become ordered. Since J_{3z} is the interaction between spins from the same sublattice, a ferromagnetic J_{3z} would simply favor $\mathbf{Q} = (000)$, even though the four spins on each tetrahedron of the pyrochlore lattice obey the "2-in–2-out" ice rule [see Fig. 2(a) of the main text]. Since this $\mathbf{Q} = (000)$ is not proximate to the U(1) QSL phase, we expect

a *strongly first-order* transition as we increase $|J_{3z}/J_z|$ for a ferromagnetic J_{3z}.

For an antiferromagnetic J_{3z}, although the Luttinger-Tisza method gives a continuous line degeneracy for the ordering wave vector, the Ising constraint immediately select the collinear order with an ordering wave vector $\mathbf{Q} = 2\pi(001)$. As we show in the main text, this Ising order is proximate to the U(1) QSL via a monopole condensation transition. Therefore, we expect either a continuous transition or an extremely weakly first-order transition driven by fluctuations as we increase $|J_{3z}/J_z|$ for an antiferromagnetic J_{3z}.

In the future, it would be interesting to implement a large-scale QMC simulation of the model in Eq. (D1) to confirm the monopole condensation transition out the QSI U(1) QSL.

Finally, we propose a perturbative version of the model in Eq. (D1). The new model includes the ring exchange on the pyrochlore hexagons and the third-neighbor Ising exchange and is given as

$$H_2 = -\sum_{\hexagon_p} \frac{K}{2}(\tau_1^+\tau_2^-\tau_3^+\tau_4^-\tau_5^+\tau_6^- + \text{H.c.}) + \sum_{\langle\langle\langle ij\rangle\rangle\rangle} J_{3z}\tau_i^z\tau_j^z, \tag{D2}$$

and we further restrict the Hilbert space to be the "2-in–2-out" ice manifold. Therefore, this new Hamiltonian will only act on the states in the ice manifold. This perturbative model was already proposed in one perturbative limit of the realistic spin model for $Yb_2Ti_2O_7$ in Ref. [38]. When $|J_{3z}| \ll K$, the ground state of H_2 is the QSI U(1) QSL phase. When $|J_{3z}| \gg K$, the system develops $\mathbf{Q} = 2\pi(001)$ antiferromagnetic order for a positive J_{3z}, and $\mathbf{Q} = (000)$ ferromagnetic order for a negative J_{3z}. Again, we expect the transition from the QSI U(1) QSL to the ferromagnetic state is strongly first order, while the transition to the antiferromagnetic state is either continuous or extremely weakly first order.

[1] D. Yanagishima and Y. Maeno, Metal-nonmetal changeover in pyrochlore iridates, J. Phys. Soc. Jpn. **70**, 2880 (2001).

[2] K. Matsuhira, M. Wakeshima, R. Nakanishi, T. Yamada, A. Nakamura, W. Kawano, S. Takagi, and Y. Hinatsu, Metal-insulator Transition in Pyrochlore Iridates $Ln_2Ir_2O_7$ (Ln = Nd, Sm, and Eu), J. Phys. Soc. Jpn. **76**, 043706 (2007).

[3] D. Pesin and L. Balents, Mott physics and band topology in materials with strong spin-orbit interaction, Nat. Phys. **6**, 376 (2010).

[4] B.-J. Yang and Y. B. Kim, Topological insulators and metal-insulator transition in the pyrochlore iridates, Phys. Rev. B **82**, 085111 (2010).

[5] X. Wan, A. M. Turner, A. Vishwanath, and S. Y. Savrasov, Topological semimetal and Fermi-arc surface states in the electronic structure of pyrochlore iridates, Phys. Rev. B **83**, 205101 (2011).

[6] W. Witczak-Krempa and Y. B. Kim, Topological and magnetic phases of interacting electrons in the pyrochlore iridates, Phys. Rev. B **85**, 045124 (2012).

[7] G. Chen and M. Hermele, Magnetic orders and topological phases from f-d exchange in pyrochlore iridates, Phys. Rev. B **86**, 235129 (2012).

[8] P. Goswami, B. Roy, and S. Das Sarma, Itinerant spin ice order, Weyl metal, and anomalous Hall effect in $Pr_2Ir_2O_7$, arXiv:1603.02273.

[9] E.-G. Moon, C. Xu, Y. B. Kim, and L. Balents, Non-Fermi-Liquid and Topological States with Strong Spin-Orbit Coupling, Phys. Rev. Lett. **111**, 206401 (2013).

[10] S. Nakatsuji, Y. Machida, Y. Maeno, T. Tayama, T. Sakakibara, J. van Duijn, L. Balicas, J. N. Millican, R. T. Macaluso, and J. Y. Chan, Metallic Spin-Liquid Behavior of the Geometrically Frustrated Kondo Lattice $Pr_2Ir_2O_7$, Phys. Rev. Lett. **96**, 087204 (2006).

[11] Y. Machida, S. Nakatsuji, Y. Maeno, T. Tayama, T. Sakakibara, and S. Onoda, Unconventional Anomalous Hall Effect Enhanced by a Noncoplanar Spin Texture in the Frustrated Kondo Lattice $Pr_2Ir_2O_7$, Phys. Rev. Lett. **98**, 057203 (2007).

[12] Y. Machida, S. Nakatsuji, S. Onoda, T. Tayama, and T. Sakakibara, Time-reversal symmetry breaking and spontaneous Hall effect without magnetic dipole order, Nature (London) **463**, 210 (2009).

[13] D. E. MacLaughlin, O. O. Bernal, L. Shu, J. Ishikawa, Y. Matsumoto, J.-J. Wen, M. Mourigal, C. Stock, G. Ehlers, C. L. Broholm, Yo Machida, K. Kimura, S. Nakatsuji, Y. Shimura, and T. Sakakibara, Unstable spin-ice order in the stuffed metallic pyrochlore $Pr_{2+x}Ir_{2-x}O_{7-\delta}$, Phys. Rev. B **92**, 054432 (2015).

[14] W. Witczak-Krempa, G. Chen, Y. B. Kim, and L. Balents, Correlated quantum phenomena in the strong spin-orbit regime, Annu. Rev. Condens. Matter Phys. **5**, 57 (2014).

[15] R. Flint and T. Senthil, Chiral RKKY interaction in $Pr_2Ir_2O_7$, Phys. Rev. B **87**, 125147 (2013).

[16] S. Lee, A. Paramekanti, and Y. B. Kim, RKKY Interactions and the Anomalous Hall Effect in Metallic Rare-Earth Pyrochlores, Phys. Rev. Lett. **111**, 196601 (2013).

[17] Z. Tian, Y. Kohama, T. Tomita, H. Ishizuka, T. H. Hsieh, J. J. Ishikawa, K. Kindo, L. Balents, and S. Nakatsuji, Field-induced quantum metal-insulator transition in the pyrochlore iridate $Nd_2Ir_2O_7$, Nat. Phys. **12**, 134 (2016).

[18] M. Hermele, M. P. A. Fisher, and L. Balents, Pyrochlore photons: The $U(1)$ spin liquid in a $S = \frac{1}{2}$ three-dimensional frustrated magnet, Phys. Rev. B **69**, 064404 (2004).

[19] H. R. Molavian, M. J. P. Gingras, and B. Canals, Dynamically Induced Frustration as a Route to a Quantum Spin Ice State in $Tb_2Ti_2O_7$ via Virtual Crystal Field Excitations and Quantum Many-Body Effects, Phys. Rev. Lett. **98**, 157204 (2007).

[20] D. A. Huse, W. Krauth, R. Moessner, and S. L. Sondhi, Coulomb and Liquid Dimer Models in Three Dimensions, Phys. Rev. Lett. **91**, 167004 (2003).

[21] L. Savary and L. Balents, Quantum spin liquids, arXiv:1601.03742.

[22] K. Ross, L. Savary, B. Gaulin, and L. Balents, Quantum Excitations in Quantum Spin Ice, Phys. Rev. X **1**, 021002 (2011).

[23] K. Kimura, K. Nakatsuji, J.-J. Wen, C. Broholm, M. B. Stone, E. Nishibori, and H. Sawa, Quantum fluctuations in spin-ice-like $Pr_2Zr_2O_7$, Nat. Commun. **4**, 2914 (2013).

[24] L.-J. Chang, S. Onoda, Y. Su, Y.-J. Kao, K.-D. Tsuei, Y. Yasui, K. Kakurai, and M. R. Lees, Higgs transition from a magnetic Coulomb liquid to a ferromagnet in $Yb_2Ti_2O_7$, Nat. Commun. **3**, 992 (2012).

[25] Y. Wan and O. Tchernyshyov, Quantum Strings in Quantum Spin Ice, Phys. Rev. Lett. **108**, 247210 (2012).

[26] J. S. Gardner, S. R. Dunsiger, B. D. Gaulin, M. J. P. Gingras, J. E. Greedan, R. F. Kiefl, M. D. Lumsden, W. A. MacFarlane, N. P. Raju, J. E. Sonier, I. Swainson, and Z. Tun, Cooperative Paramagnetism in the Geometrically Frustrated Pyrochlore Antiferromagnet $Tb_2Ti_2O_7$, Phys. Rev. Lett. **82**, 1012 (1999).

[27] O. Benton, O. Sikora, and N. Shannon, Seeing the light: Experimental signatures of emergent electromagnetism in a quantum spin ice, Phys. Rev. B **86**, 075154 (2012).

[28] G. Chen, H.-Y. Kee, and Y. B. Kim, Fractionalized charge excitations in a spin liquid on partially filled pyrochlore lattices, Phys. Rev. Lett. **113**, 197202 (2014).

[29] T. Fennell, M. Kenzelmann, B. Roessli, M. K. Haas, and R. J. Cava, Power-Law Spin Correlations in the Pyrochlore Antiferromagnet $Tb_2Ti_2O_7$, Phys. Rev. Lett. **109**, 017201 (2012).

[30] K. C. Rule, J. P. C. Ruff, B. D. Gaulin, S. R. Dunsiger, J. S. Gardner, J. P. Clancy, M. J. Lewis, H. A. Dabkowska, I. Mirebeau, P. Manuel, Y. Qiu, and J. R. D. Copley, Field-Induced Order and Spin Waves in the Pyrochlore Antiferromagnet $Tb_2Ti_2O_7$, Phys. Rev. Lett. **96**, 177201 (2006).

[31] Y.-D. Li and G. Chen, Octupolar quantum spin ice: Controlling spinons in a U(1) quantum spin liquid, arXiv:1607.02287.

[32] S. T. Bramwell and M. J. P. Gingras, Spin Ice State in Frustrated Magnetic Pyrochlore Materials, Science **294**, 1495 (2001).

[33] M. J. Harris, S. T. Bramwell, D. F. McMorrow, T. Zeiske, and K. W. Godfrey, Geometrical Frustration in the Ferromagnetic Pyrochlore $Ho_2Ti_2O_7$, Phys. Rev. Lett. **79**, 2554 (1997).

[34] C. Castelnovo1, R. Moessner, and S. L. Sondhi, Magnetic monopoles in spin ice, Nature (London) **451**, 42 (2008).

[35] J. S. Gardner, M. J. P. Gingras, and J. E. Greedan, Magnetic pyrochlore oxides, Rev. Mod. Phys. **82**, 53 (2010).

[36] M. J. P. Gingras and P. A. McClarty, Quantum spin ice: A search for gapless quantum spin liquids in pyrochlore magnets, Rep. Prog. Phys. **77**, 056501 (2014).

[37] Z. Hao, A. G. R. Day, and M. J. P. Gingras, Bosonic many-body theory of quantum spin ice, Phys. Rev. B **90**, 214430 (2014).

[38] L. Savary and L. Balents, Coulombic Quantum Liquids in Spin-1/2 Pyrochlores, Phys. Rev. Lett. **108**, 037202 (2012).

[39] S. Lee, S. Onoda, and L. Balents, Generic quantum spin ice, Phys. Rev. B **86**, 104412 (2012).

[40] Y.-P. Huang, G. Chen, and M. Hermele, Quantum Spin Ices and Topological Phases from Dipolar-Octupolar Doublets on the Pyrochlore Lattice, Phys. Rev. Lett. **112**, 167203 (2014).

[41] Y. Yasui, M. Soda, S. Iikubo, M. Ito, M. Sato, N. Hamaguchi, T. Matsushita, N. Wada, T. Takeuchi, N. Aso, and K. Kakurai, Ferromagnetic Transition of Pyrochlore Compound $Yb_2Ti_2O_7$, J. Phys. Soc. Jpn. **72**, 3014 (2003).

[42] L.-J. Chang, M. R. Lees, I. Watanabe, A. D. Hillier, Y. Yasui, and S. Onoda, Static magnetic moments revealed by muon spin relaxation and thermodynamic measurements in the quantum spin ice $Yb_2Ti_2O_7$, Phys. Rev. B **89**, 184416 (2014).

[43] E. Lhotel, S. R. Giblin, M. R. Lees, G. Balakrishnan, L. J. Chang, and Y. Yasui, First-order magnetic transition in $Yb_2Ti_2O_7$, Phys. Rev. B **89**, 224419 (2014).

[44] L. Savary, X. Wang, H.-Y. Kee, Y. B. Kim, Y. Yu, and G. Chen, Quantum spin ice on the breathing pyrochlore lattice, Phys. Rev. B **94**, 075146 (2016).

[45] E. Fradkin and S. H. Shenker, Phase diagrams of lattice gauge theories with Higgs fields, Phys. Rev. D **19**, 3682 (1979).

[46] R. Savit, Duality in field theory and statistical systems, Rev. Mod. Phys. **52**, 453 (1980).

[47] C. Dasgupta and B. I. Halperin, Phase transition in a lattice model of superconductivity, Phys. Rev. Lett. **47**, 1556 (1981).

[48] M. E Peskin, Mandelstam-'t hooft duality in abelian lattice models, Ann. Phys. (NY) **113**, 122 (1978).

[49] D. L. Bergman, G. A. Fiete, and L. Balents, Ordering in a frustrated pyrochlore antiferromagnet proximate to a spin liquid, Phys. Rev. B **73**, 134402 (2006).

[50] O. I. Motrunich and T. Senthil, Origin of artificial electrodynamics in three-dimensional bosonic models, Phys. Rev. B **71**, 125102 (2005).

[51] X.-G. Wen, Quantum orders and symmetric spin liquids, Phys. Rev. B **65**, 165113 (2002).

[52] B. I. Halperin, T. C. Lubensky, and S.-k. Ma, First-Order Phase Transitions in Superconductors and Smectic-*A* Liquid Crystals, Phys. Rev. Lett. **32**, 292 (1974).

[53] E. Berg, E. Fradkin, and S. A Kivelson, Charge-4e superconductivity from pair-density-wave order in certain high-temperature superconductors, Nat. Phys. **5**, 830 (2009).

[54] P. A. Lee, Amperean Pairing and the Pseudogap Phase of Cuprate Superconductors, Phys. Rev. X **4**, 031017 (2014).

[55] L. Savary and L. Balents, Spin liquid regimes at nonzero temperature in quantum spin ice, Phys. Rev. B **87**, 205130 (2013).

[56] Y. Tokiwa, J. J. Ishikawa, S. Nakatsuji, and P. Gegenwart, Quantum criticality in a metallic spin liquid, Nat. Mater. **13**, 356359 (2014).

[57] Y.-D. Li and G. Chen (unpublished).

[58] T. Kondo, M. Nakayama, R. Chen, J. J. Ishikawa, E.-G. Moon, T. Yamamoto, Y. Ota, W. Malaeb, H. Kanai, Y. Nakashima *et al.*, Quadratic Fermi node in a 3D strongly correlated semimetal, Nat. Commun. **6**, 10042 (2015).

[59] H. v. Löhneysen, A. Rosch, M. Vojta, and P. Wölfle, Fermi-liquid instabilities at magnetic quantum phase transitions, Rev. Mod. Phys. **79**, 1015 (2007).

[60] E. Fradkin, *Field Theories of Condensed Matter Physics*, 2nd ed. (Cambridge University Press, Cambridge, 2013).

[61] R. Moessner, S. L. Sondhi, and E. Fradkin, Short-ranged resonating valence bond physics, quantum dimer models, and ising gauge theories, Phys. Rev. B **65**, 024504 (2001).

[62] T. Senthil and M. P. A. Fisher, Z_2 gauge theory of electron fractionalization in strongly correlated systems, Phys. Rev. B **62**, 7850 (2000).

[63] C. Xu and L. Balents, Quantum phase transitions around the staggered valence-bond solid, Phys. Rev. B **84**, 014402 (2011).

[64] K. Fritsch, E. Kermarrec, K. A. Ross, Y. Qiu, J. R. D. Copley, D. Pomaranski, J. B. Kycia, H. A. Dabkowska, and B. D. Gaulin, Temperature and magnetic field dependence of spin-ice correlations in the pyrochlore magnet $Tb_2Ti_2O_7$, Phys. Rev. B **90**, 014429 (2014).

[65] Y. Matsuda (unpublished).

[66] A. Banerjee, S. V. Isakov, K. Damle, and Y. B. Kim, Unusual liquid state of hard-core bosons on the pyrochlore lattice, Phys. Rev. Lett. **100**, 047208 (2008).

[67] J.-P. Lv, G. Chen, Y. Deng, and Z. Y. Meng, Coulomb Liquid Phases of Bosonic Cluster Mott Insulators on a Pyrochlore Lattice, Phys. Rev. Lett. **115**, 037202 (2015).

[68] Y. Kato and S. Onoda, Numerical evidence of quantum melting of spin ice: Quantum-to-classical crossover, Phys. Rev. Lett. **115**, 077202 (2015).